

# Evaluating along-strike variation using thin-bedded facies analysis, Upper Cretaceous Ferron Notom Delta, Utah

ZHIYANG LI\*, JANOK BHATTACHARYA† and JUERGEN SCHIEBER\*

\*Department of Geological Sciences, Indiana University Bloomington, 1001 East 10th Street, Bloomington, Indiana, 47405-1405, USA (E-mails: zl29@iu.edu, lizhiyanglee@gmail.com)

†School of Geography and Earth Sciences, McMaster University, 1280 Main Street West, Hamilton, Ontario, Canada L8S 4L8

Associate Editor – Gary Hampson

## ABSTRACT

Thin-bedded delta-front and prodelta facies of the Upper Cretaceous Ferron Notom Delta Complex near Hanksville in southern Utah, USA, show significant along-strike facies variability. Primary initiation processes that form these thin beds include surge-type turbidity currents, hyperpycnal flows and storm surges. The relative proportion of sedimentary structures generated by each of these depositional processes/events has been calculated from a series of measured sedimentological sections within a single parasequence (PS6–1) which is exposed continuously along depositional strike. For each measured section, sedimentological data including grain size, lithology, bedding thickness, sedimentary structures and ichnological suites have been documented. Parasequence 6–1 shows a strong along-strike variation with a wave-dominated environment in the north, passing abruptly into a fluvial-dominated area, then to an environment with varying degrees of fluvial and wave influence southward, and back to a wave-dominated environment further to the south-east. The lateral facies variations integrated with palaeocurrent data indicate that parasequence 6–1 is deposited as a storm-dominated symmetrical delta with a large river-dominated bayhead system linked to an updip fluvial feeder valley. This article indicates that it is practical to quantify the relative importance of depositional processes and determine the along-strike variation within an ancient delta system using thin-bedded facies analysis. The wide range of vertical stratification and grading sequences present in these event beds also allows construction of conceptual models of deposition from turbidity currents (i.e. surge-type turbidity currents and hyperpycnal flows) and storm surges, and shows that there are significant interactions and linkages of these often paired processes.

**Keywords** Along-strike variation, Ferron Notom Delta, hyperpycnal flows, prodelta, storms, thin beds.

## INTRODUCTION

The traditional tripartite classification of deltas into fluvial-dominated, wave-dominated and tide-dominated end-members was based on the relative influence of river input, waves and tides, as well as the plan-view geometries of deltaic

sand bodies (Coleman & Wright, 1975; Galloway, 1975). Since then, many other parameters, such as type of feeder system, water depth and type of mouth-bar process, have been incorporated to expand this ternary classification (Reading & Collinson, 1996). However, these classification schemes deal poorly with the internal facies

complexities within ancient deltaic systems, because most deltaic systems are mixed-process systems that have been influenced by rivers, waves and tides to varying degrees at the same time (Gani & Bhattacharya, 2007; Ainsworth *et al.*, 2011). The degree of influence of these processes is hypothesized to change with along-strike position. In addition, prodelta facies may be less re-worked by fair-weather waves, compared with sandy delta-front deposits, and thus the prodelta deposits may contain a better record of storms and river flood events. Traditional deltaic facies models also tend to focus on the sandy parts of systems and general trends, such as overall coarsening upward, versus bed by bed detail of sedimentary processes in the muddier parts of such systems. As a consequence, few studies have documented the bed-scale facies variation in prodeltaic facies through time and space within a mixed-influence deltaic system.

Recent spatially focused facies-oriented studies on both modern and ancient deltaic systems may be more effective in revealing the inherent complexity of delta-building processes, compared with the traditional tripartite delta classification. For example, in a plan-view study of modern wave-influenced deltas, the concept of delta asymmetry was developed, suggesting that where there is a dominant direction of longshore currents generated by oblique wave approach, the resulting delta shows a more wave-dominated updrift side, and a more fluvial-dominated downdrift side (Bhattacharya & Giosan, 2003). These concepts have been applied in a number of ancient examples using both well-log, core and/or outcrop data, in which the organization and proportion of internal facies architectural elements within the prodelta and delta-front deposits show a systematic along-strike variation among wave, tidal and fluvial processes (Hampson & Storms, 2003; Hampson, 2005; Coates & MacEachern, 2007; Gani & Bhattacharya, 2007; Hansen, 2007; Charvin *et al.*, 2010; Dafoe *et al.*, 2010; Fielding, 2010; Hampson *et al.*, 2011; Li *et al.*, 2011; Buatois *et al.*, 2012).

Because depositional processes are the first-order controls on the internal facies complexity within deltaic systems, Ainsworth *et al.* (2011) provided a semi-quantitative process-based classification scheme to determine the dominant and subordinate processes in both modern and ancient delta systems. In a modern deltaic system, the depositional elements/facies generated from fluvial-dominated, wave-dominated and

tide-dominated processes can be identified and, by calculating the area covered by each element in plan view, the corresponding relative proportion of each depositional process can be determined (Ainsworth *et al.*, 2011). Similar concepts can be applied to ancient systems, using either core or outcrop data. The assumption is that dominant depositional processes would produce the largest proportion of sedimentary structures and will have a greater chance to be preserved in the rock record. Calculating the percentage of sedimentary structures generated by different depositional processes thus allows determination of the relative importance of these different depositional processes and a more quantitative process classification delta depositional system.

Prodelta units, which are typically thin-bedded or laminated, are also typically deposited below fair-weather wave-base, and are more likely to record primary depositional processes or reworking by storms, versus sandier delta-front and shoreface deposits, which may experience greater reworking by fair-weather processes. As a consequence, there is a preservational bias in shallower sandy facies to reworking of sediment by fair-weather waves and tides, as opposed to the initial delivery mechanism, which may be better recorded in the prodelta. Most deposition in the prodelta takes place during river floods and storm events (Mulder & Syvitski, 1995; Myrow *et al.*, 2008).

Primary formative processes of the thin-bedded prodelta deposits include surge-type turbidity currents, hyperpycnal flows and storm surges (Normark & Piper, 1991; Mulder & Syvitski, 1995; Myrow *et al.*, 2008; Lock *et al.*, 2009). Several recent studies have been conducted to investigate the variations in depositional processes in deltaic systems by examining the prodelta deposits along depositional dip. Based on detailed facies analyses of the event beds from the prodelta units in the Minturn Formation, Lamb *et al.* (2008) illustrated variations in the relative influence between turbidity currents and storm surges from proximal to distal settings. These studies suggest that the variability shown in the mud-dominated prodelta facies may directly reflect the dominant sediment delivery processes (Schieber, 1999; Lamb *et al.*, 2008; Myrow *et al.*, 2008; MacQuaker *et al.*, 2010). However, only a few studies have analysed thin-bedded prodelta facies in detail to evaluate along-strike variations in depositional processes within

ancient deltaic systems (Plint, 2014). The lack of such studies is mainly due to: (i) mud-dominated prodelta facies are commonly overlooked because the fine-grained deposits are thought to have poorer reservoir quality and therefore attract much less attention when compared with the sandy facies (Ainsworth *et al.*, 2011); (ii) thin-bed investigation requires highly detailed analysis (millimetre to centimetre-scale) to fully describe the thin-bedded prodelta facies, and this can be very time-consuming (Schieber, 1999; Bhattacharya & MacEachern, 2009; Seepersad, 2012; Plint, 2014); (iii) outcrop and core data from thin-bedded units may be limited in availability, and subsequent weathering of mudstones, particularly in outcrop, may preclude such detailed analysis; and (iv) there may be uncertainties regarding the linkage between the flow characteristics of the primary formative processes (i.e. surge-type turbidity currents, hyperpycnal flows and storm surges), as well as interactions between turbidity currents and storm surges (Stow & Shanmugam, 1980; Myrow *et al.*, 2002; Mulder *et al.*, 2003; Lamb *et al.*, 2008; Lamb & Mohrig, 2009; Talling *et al.*, 2012; Plint, 2014).

The primary objectives of the present study are two-fold: (i) to evaluate the along-strike variation in this ancient deltaic system based on millimetre to centimetre-scale sedimentological analysis of the prodelta facies within a parasequence (parasequence 6–1); and (ii) to summarize the typical grain-size grading patterns and typical vertical sequences of sedimentary structures present in the event beds, especially those that allow the distinction of formative mechanisms.

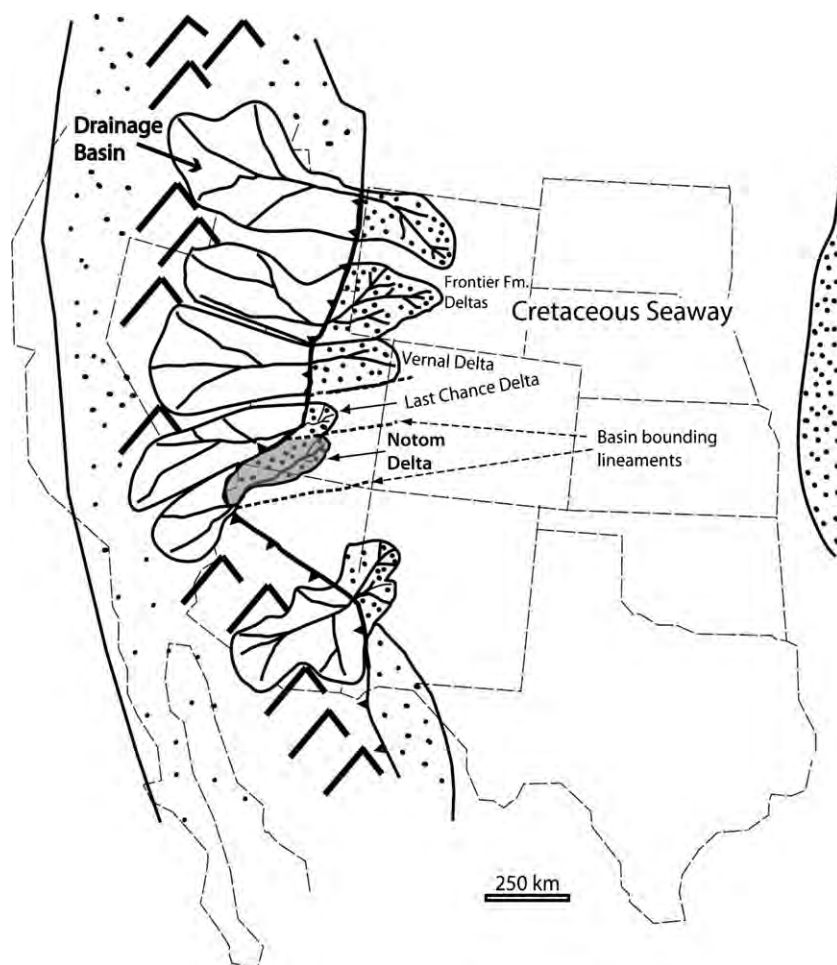
## GEOLOGICAL SETTING AND STUDY AREA

The Ferron Sandstone Member was deposited during the Middle to Late Cretaceous in the Western Interior Seaway (Bhattacharya & Tye, 2004). It lies on top of the Tununk Shale Member and is overlain by the Blue Gate Shale Member. During overall regression, three clastic wedges constituting the Ferron Sandstone were deposited along the western margin of the Cretaceous epeiric seaway: these are informally named the Vernal, Last Chance and Notom delta systems (Fig. 1).

Regional palaeogeographic reconstructions (Slingerland *et al.*, 1996; Bhattacharya & Tye, 2004) indicate that the Ferron Notom delta

was fed by a trunk river draining highlands in the south-west and prograding towards the north-east (Fig. 1). Palaeoenvironmental reconstructions of the Western Interior Seaway, based on numerical simulations, suggest that circulation in the seaway was storm-dominated during deposition of the Ferron Sandstone Member, and that longshore currents and net sediment drift were predominantly directed to the south along the western side of the seaway (Barron, 1989; Ericksen & Slingerland, 1990; Slingerland & Keen, 1999). Therefore, the Ferron Notom delta experienced relatively high sediment load from the nearby orogenic belt, and prograded north-eastward into a storm-dominated seaway, where the strong longshore currents deflected the sediment to the south (Fielding, 2010). Previous studies suggest that the Ferron Notom delta was exposed to both strong fluvial and storm influence (Ericksen & Slingerland, 1990; Slingerland & Keen, 1999; Bhattacharya & MacEachern, 2009; Li *et al.*, 2011). The distal delta-front and prodelta facies (or the lower shoreface and offshore facies) consist largely of thin beds (Passey *et al.*, 2006).

A detailed sequence stratigraphic framework of the Ferron Notom delta based on the outcrops located in south-central Utah (Fig. 2) indicates that it consists of 43 parasequences, 18 parasequence sets and six sequences (Li *et al.*, 2010; Zhu *et al.*, 2012, fig. 15). The present study is focused on parasequence set 6 (PS6), which was deposited during a forced regression associated with a relative sea-level fall and linked to an updip valley in Sequence 2 (Zhu *et al.*, 2012). Previous studies indicate that PS6 contains both river-dominated and wave-dominated facies (Li *et al.*, 2010, 2011; Ahmed *et al.*, 2014) and shows strong lateral facies variations along depositional strike (Fig. 3). Previous depositional models of PS6 were derived based mostly on the facies characteristics shown in the sandy facies, whereas the variability displayed in the mud-dominated prodelta facies has not been evaluated to the same degree. Parasequence set 6 is further subdivided into three individual parasequences PS6–1, PS6–2 and PS6–3 (Fig. 3). This article focuses on PS6–1, which is continuously exposed along depositional strike in the study area, and therefore provides an opportunity to document the complex lateral variability between dominant depositional processes recorded in the internal facies. Twelve detailed



**Fig. 1.** Palaeogeographic reconstruction showing the location of the Western Interior Seaway and delta complexes of the Ferron Sandstone Member of the Mancos Shale Formation. The Notom Delta is highlighted in grey (modified from Bhattacharya & Tye, 2004).

sedimentological sections of the thin-bedded prodelta and heterolithic delta-front facies have been measured along depositional strike in order to quantify the lateral facies and process variability (Fig. 2).

## METHODOLOGY

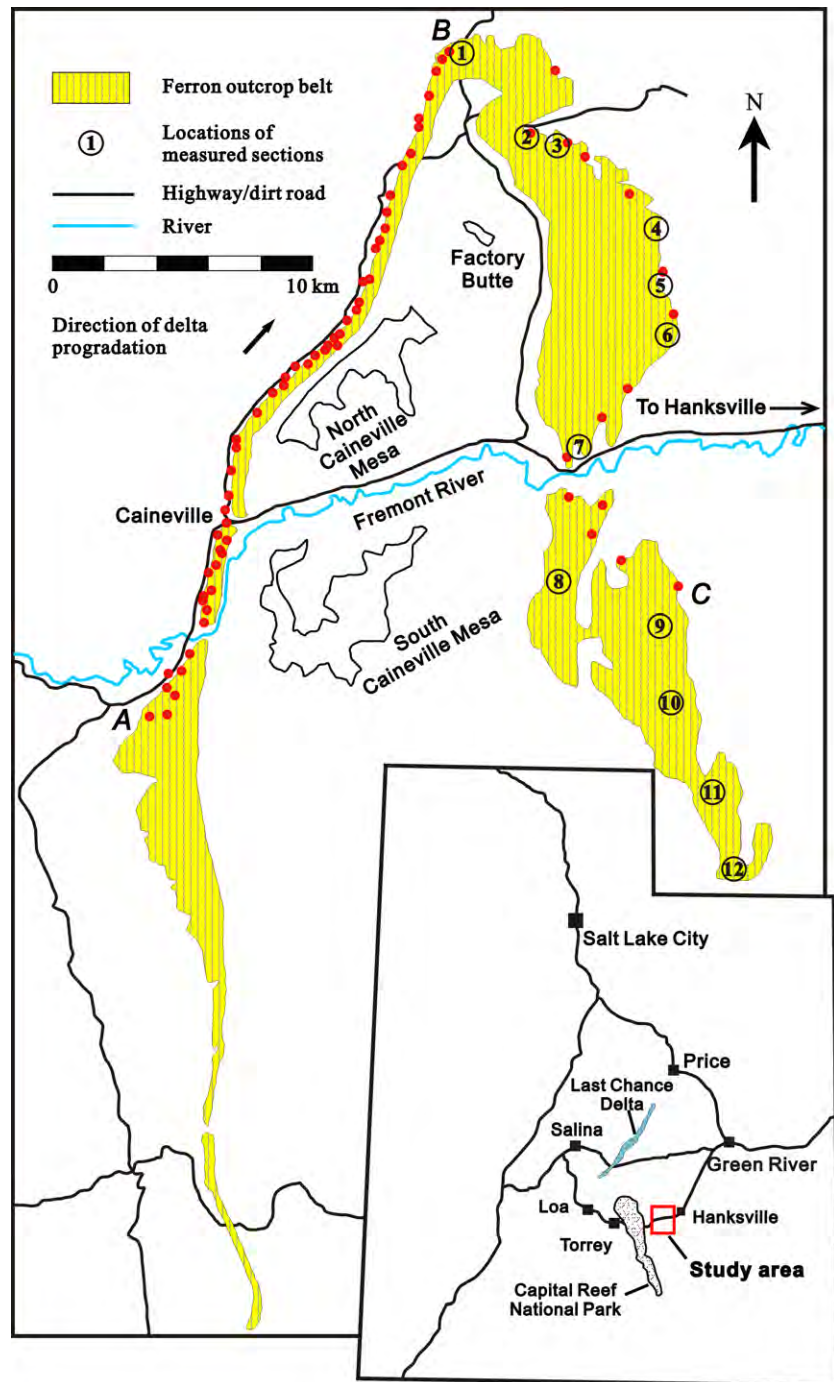
### Thin-bedded facies analysis

Twelve sedimentological sections of the thin-bedded facies were measured along depositional strike within PS6–1. The term ‘thin bed’ is generally used to describe beds with a thickness ranging from 3 to 10 cm (Campbell, 1967; Passey *et al.*, 2006). In the present study, beds measured in the prodelta and distal delta-front facies range in thickness from as small as 1 mm to as large as 50 cm, although the thickness of most beds ranges from several millimetres to a few centimetres. Most sections were measured in

well-exposed outcrops, where weathering was minimal. In places, small trenches were dug in order to expose the lower part of the prodelta facies. For each bed measured in this study, important sedimentological data were collected, including grain size, bedding thickness, sedimentary structures, palaeocurrent data, bioturbation intensity and ichnological suites. Thirty-one rock samples were collected to describe detailed facies characteristics in polished slabs and thin sections. Each measured section included *ca* 150 or more thin beds, and a total of *ca* 3500 beds were thus described. For example, 480 thin beds have been measured in section 4 which has a total thickness of 6.2 m. The thickness of each thin bed measured in section 4 ranges from 0.1 to 25.5 cm, with an average bed thickness of 1.3 cm.

In this study, the fine-grained mudstone and siltstone were classified into five categories: clayey mudstone (80% clay + 20% silt), silty mudstone (60% clay + 40% silt), mudstone (50% clay + 50% silt), muddy siltstone (40%

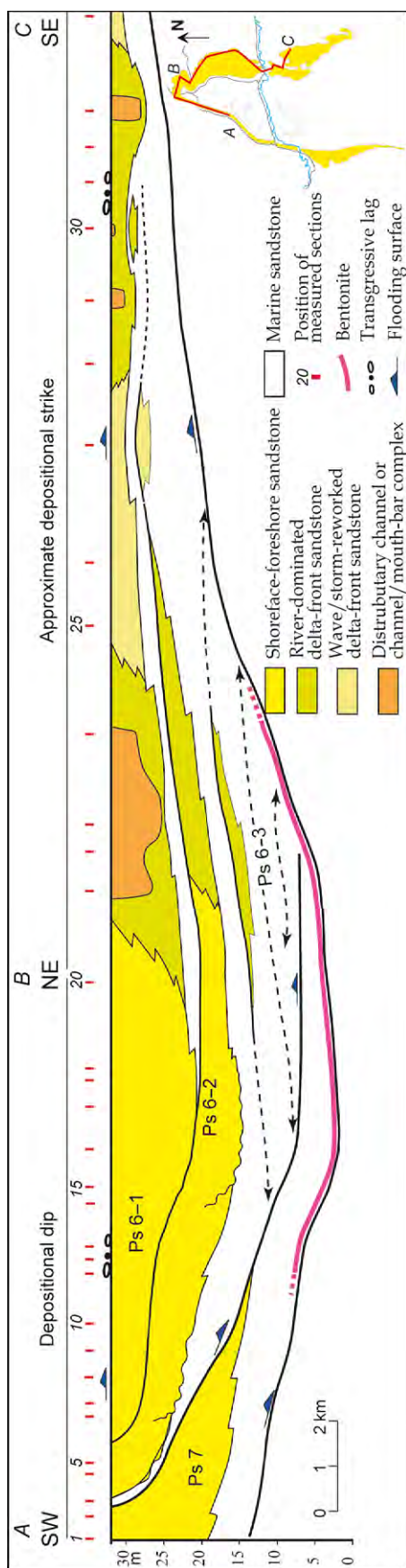




**Fig. 2.** Location of the Ferron Sandstone outcrop belts between Hanksville and Caineville. Red dots between 'A' and 'B' indicate the locations of all dip sections (Zhu *et al.*, 2012). Red dots between 'B' and 'C' are locations of all strike sections (Li *et al.*, 2011). Black circles with numbers indicate the locations of all the sections measured in this study.

clay + 60% silt) and siltstone (20% clay + 80% silt). The variations in the grain size of mudstone and siltstone were determined by: (i) petrographic study of rock samples under the microscope; (ii) feeling and chewing rock samples to estimate silt versus clay content; and (iii) variations in colour. Beds containing higher percentages of clay-size grains appear dark grey to black, whereas beds containing higher amounts

of silt-size grains are lighter grey. Detailed differentiation of grain size helps to determine the grading patterns of beds formed from a single depositional event. Although petrographic analysis is more accurate compared to the other two methods, it would be extremely time-consuming and expensive to estimate the clay content in every thin bed under the microscope. Therefore, in this study, the clay content



**Fig. 3.** Regional cross-section of parasequence set 6 (Li *et al.*, 2011). Location of regional cross-section is shown by the red line along outcrop belt ('A'–'B'–'C'). This study focuses on the thin-bedded facies in the youngest parasequence 6–1. Note that the sandy facies in parasequence 6–1 show strong along-strike variation from the wave-dominated shoreface deposits in the north passing into fluvial-dominated, wave-influenced facies towards the south.

of most beds is measured using the two latter methods in the field. Observations of thin sections from specific thin beds can help to calibrate these results.

Sedimentary structures within each bed were recognized and recorded mainly on the outcrop, and some small-scale sedimentary structures were also identified in polished rock samples and thin sections. In addition, palaeocurrent data were recorded, including dip directions of foresets in current ripples and combined-flow ripples. The strike direction of wave-ripple crests was also noted.

The Bioturbation Index (BI) of Taylor & Goldring (1993) is used to depict the intensity of bioturbation in the sediments. By connecting all the bioturbation intensities of all the beds in one measured section using a continuous line curve (i.e. the 'BI log' as suggested by Gani *et al.*, 2008), the vertical and lateral variation in bioturbation intensity can be readily evaluated.

By combining the grain-size grading patterns, vertical stratification of sedimentary structures, bioturbation intensity and ichnofacies data, the depositional processes that formed these thin beds have been inferred. For each measured section, the relative percentage of facies and facies associations generated by different depositional processes has been calculated. Then the relative amount of fluvial and wave influence was determined in each measured section (Ainsworth *et al.*, 2011). By combining all 12 of the measured sections along depositional strike, the lateral variation between fluvial and wave influence within this ancient delta system is illustrated and interpreted in the context of facies models for wave-influenced deltaic systems (Bhattacharya & Giosan, 2003; Bhattacharya, 2011).

### Criteria for recognition of thin-bed processes

In deltaic systems, surge-type turbidity currents, hyperpycnal flows and storm surges are all likely to form within thin-bedded prodelta and distal delta-front facies. Surge-type turbidity currents and hyperpycnal flows indicate predominant fluvial/flood influence, and storm surges indicate strong wave/storm influence. Careful analysis of each facies and facies association is necessary to avoid misinterpretation of these depositional processes. In the next three sections, several examples of the different types of thin beds seen in the Ferron will be given, together with a description of sedimentological features and subsequent interpretation.



### Surge-type turbidity currents

Surge-type turbidity currents are generated from instantaneous slump or sediment failure, and therefore are short-lived (minutes to hours; Normark & Piper, 1991; Mulder & Syvitski, 1995; Plink-Björklund & Steel, 2004; Lamb *et al.*, 2008). During the nearly instantaneous waxing phase, the flows tend to erode. As the flow wanes, sediments deposited from these flows are characterized by a normally graded succession of bedforms reflecting waning flow energy with time, which generally are described as Bouma sequences (Bouma, 1962; Ricci Lucchi & Valmori, 1980; Stow & Shanmugam, 1980).

Although traditional Bouma sequences occur within the mud-dominated prodelta deposits of the Ferron, 'fine-grained turbidites' composed of the  $T_C$ ,  $T_D$  and  $T_E$  divisions of the Bouma sequence are common. The three-fold subdivision of  $T_E$  proposed by Piper (1978) is used in the present study to describe the fine-grained turbidite beds; these include laminated mudstone ( $T_{E-1}$ ), normally graded silty mudstone ( $T_{E-2}$ ) and structureless mudstone ( $T_{E-3}$ ). Several examples are illustrated below.

Figure 4 shows an example of a typical surge-type turbidity-current deposit. From bottom to top, two partial Bouma sequences can be seen. The lower beds show basal massive bedding ( $T_A$ ), passing into parallel bedding ( $T_B$ ) and

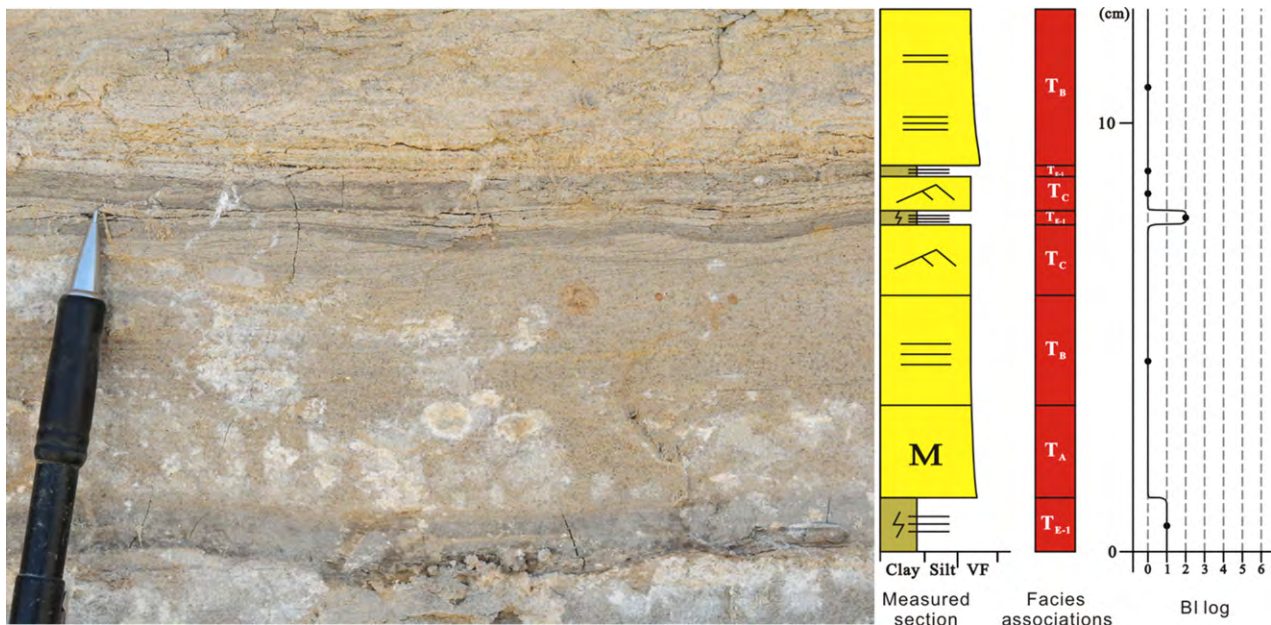
overlain by current ripple laminations ( $T_C$ ). The upper beds show incomplete Bouma sequences with very fine lower sandstone with current ripple laminations ( $T_C$ ) grading up to laminated silty mudstone ( $T_{E-1}$  units). The facies key for Fig. 4 and later diagrams is included as Fig. 5.

Figure 6 shows characteristic fine-grained Bouma-type turbidites, also from the Ferron Sandstone outcrops. Two partial fine-grained Bouma sequences can be seen in Fig. 6. The lower beds grade from laminated muddy siltstone ( $T_{E-1}$ ) to normally graded silty mudstone ( $T_{E-2}$ ). The upper beds show a complete  $T_E$  unit. The whole interval is characterized by very low BI (0 to 1), which also indicates a stressed environment due to a rapid depositional rate caused by strong fluvial influence (MacEachern *et al.*, 2005).

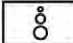



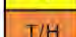


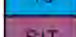

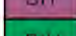

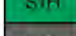
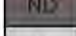
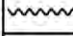
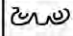
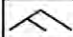

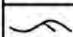

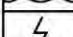

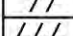
### Hyperpycnal flow

Hyperpycnites are characterized by a coarsening-upward basal unit overlain by a classical fining upward Bouma sequence resulting from waxing and waning discharge during floods, respectively (Mulder *et al.*, 2001). When the maximum flood discharge exceeds the erosion threshold, the transition between the inversely and normally graded units can be correspondingly erosional.


Figure 7 shows an example of a typical Ferron Sandstone hyperpycnite. The sandy interval



**Fig. 4.** Outcrop (photograph) showing typical Bouma  $T_A$  to  $T_C$  units and  $T_C$  to  $T_E$  units from 4.30 to 4.38 m in measured section 2 and the correlated measured section, interpreted facies associations and BI log. The pencil for scale is *ca* 1.5 cm in width. See Fig. 5 for facies key.

Sedimentary structures		Ichnofacies		Facies associations	
	Normal grading	As	<i>Asterosoma</i>		Bouma-type turbidite
	Inverse grading	Ch	<i>Chondrites</i>		Hyperpycnite
Str	Structureless mudstone	Di	<i>Diplocraterion</i>		Bouma-type turbidite/ Hyperpycnite
Un	Unknown/not available	DC	<i>Dewatering crack</i>		Tempestite
	Current ripple lamination	Fug	<i>Fugichnia</i>		Storm-influenced turbidite
	Starved ripple lamination	Op	<i>Ophiomorpha</i>		Storm-influenced hyperpycnite
	Planar lamination/bedding	Pa	<i>Paleophycus</i>		Non-deposition
M	Massive bedding	Ph	<i>Phycosiphon</i>		Unknown
	Erosional surface	PI	<i>Planolites</i>		
	Soft sedimentary deformation	Ro	<i>Rosselia</i>		
	Combined flow ripple lamination	Sch	<i>Schaubcylindrichnus</i>		
	Wave ripple lamination	Sko	<i>Skolithos</i>		
	Hummocky cross-stratification	T	<i>Terebellina</i>		
	Quasi-planar lamination	Te	<i>Teichichnus</i>		
	Slightly bioturbated: BI = 1–2	Th	<i>Thalassinoides</i>		
	Moderately bioturbated: BI = 3–4				
	Highly bioturbated: BI = 5–6				

**Grain size**



Clay – Silt – VF

Fig. 5. Facies key for the sedimentological sections presented in this study.



Fig. 6. Typical characteristics of a 'fine-grained turbidite' in outcrop. The terms T<sub>E-1</sub>, T<sub>E-2</sub> and T<sub>E-3</sub> represent laminated mudstone, normally graded mudstone and structureless mudstone, respectively (Piper, 1978). Photograph showing two amalgamated units of normally graded (indicated by red triangles) muddy siltstone from 2.79 to 2.81 m in measured section 7. The undulating dashed lines indicate erosional surfaces. See Fig. 5 for facies key.



between the bottom and top two thin beds of silty mudstone is interpreted to be deposited during one hyperpycnal flow event. Within the sandy facies, the sedimentary structures pass from the basal parallel bedding ( $T_B$ ), up to massive bedding ( $T_A$ ), then back to parallel bedding ( $T_B$ ). The grain size also shows inverse grading passing from very fine lower to very fine upper. The bed shows normal grading upward into very fine lower sandstone. Both the sequences of sedimentary structures and grain-size grading patterns indicate waxing and waning flow energy, which are interpreted to be diagnostic of hyperpycnal flows (Mulder *et al.*, 2001; Bhattacharya & MacEachern, 2009).

Figure 8 shows three typical examples of fine-grained hyperpycnite deposits in the study area. Figure 8A shows amalgamated inverse to normal grading which can be identified based on colour variation. The grain-size grading patterns can be more easily recognized on polished slabs (Fig. 8B and C). In the lower left area of Fig. 8C, the basal inverse grading unit (silty mudstone to muddy siltstone) is overlain by a normally graded unit (very fine-grained sandstone to muddy siltstone) with an erosional surface. Towards the right below the sharp surface, the basal inverse-graded unit is eroded away. The multiple stacked inverse and normally graded units (Fig. 8) could be deposited from successive hyperpycnal flows or, in some cases, from a

single hyperpycnal flow that waxed and waned (Lamb & Mohrig, 2009). The lack of burrowing between units suggests a single flood event rather than multiple flood events.

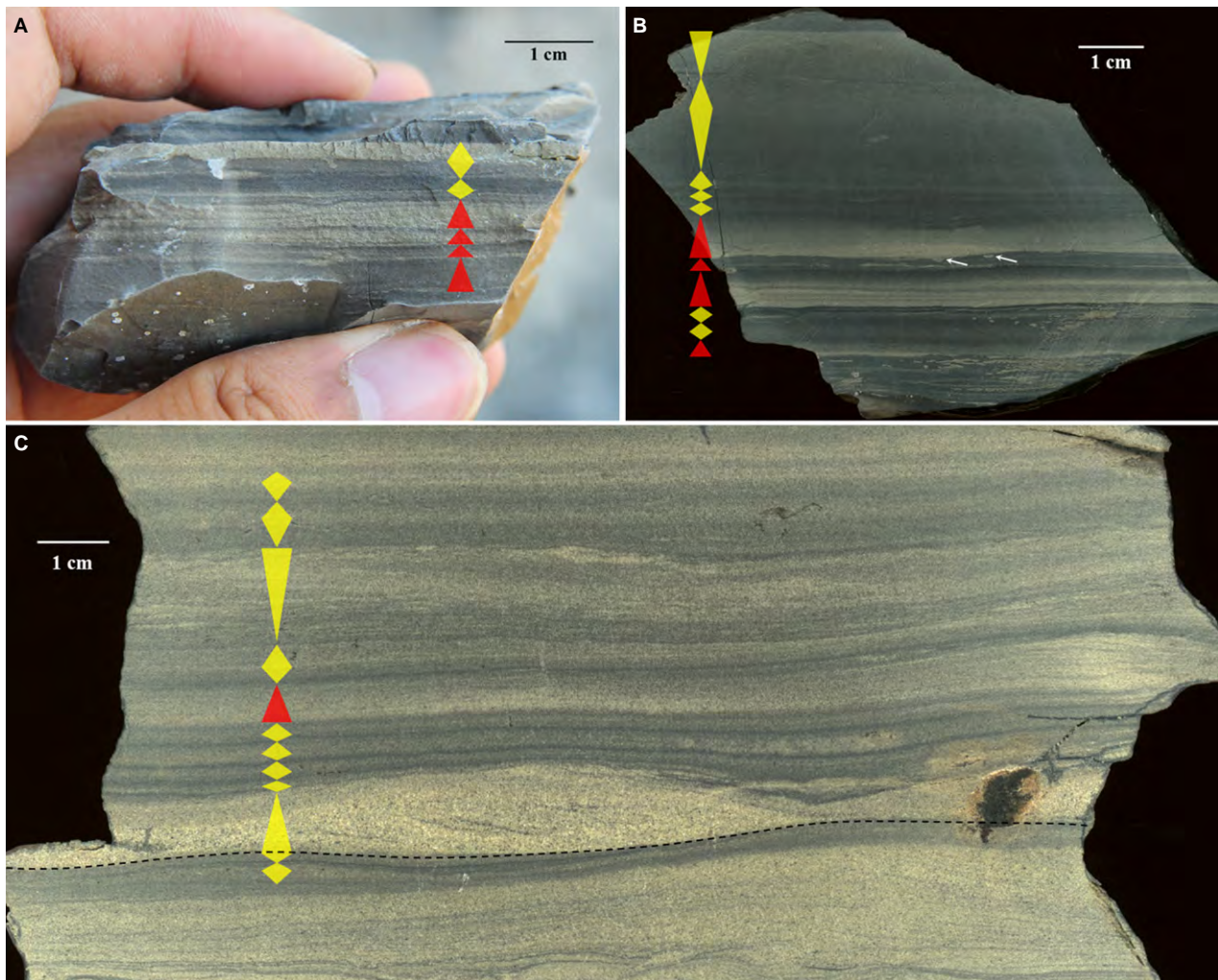
### Storm surge (tempestite)

Storm deposits (tempestites) are formed under strongly oscillatory-dominated combined-flow conditions (Swift & Nummedal, 1987; Arnott & Southard, 1990). Tempestites typically form graded beds in which parallel laminated sandstones overlie a scoured base and pass into hummocky cross-stratification (HCS) which, in turn, grades upward into smaller scale wave-ripple laminations. The tempestite may be capped by a bioturbated silt or mud drape.

Figure 9A shows a typical example of a Ferron Sandstone tempestite, in which a very fine-grained sandstone with HCS is overlain by a unit exhibiting small wave-ripple laminations. Many tempestites may show combined-flow bedforms, indicating a unidirectional component. As the unidirectional component becomes stronger, the HCS is replaced by quasi-parallel laminations (Arnott & Southard, 1990; Arnott, 1993). For example, when integrated with the well-sorted texture and the presence of typical ichnofacies, such as *Ophiomorpha* and *Skolithos*, the quasi-planar laminated very fine sandstone shown in Fig. 9B is interpreted to be deposited from oscillation-dominated combined flows.



Fig. 7. Rock sample (left-hand photograph) showing the basal coarsening-upward unit overlain by a fining upward unit from 3.80 to 3.95 m in measured section 2 and the correlated measured section, interpreted-facies associations and BI log. The pencil for scale is 13.5 cm in length. See Fig. 5 for facies key.



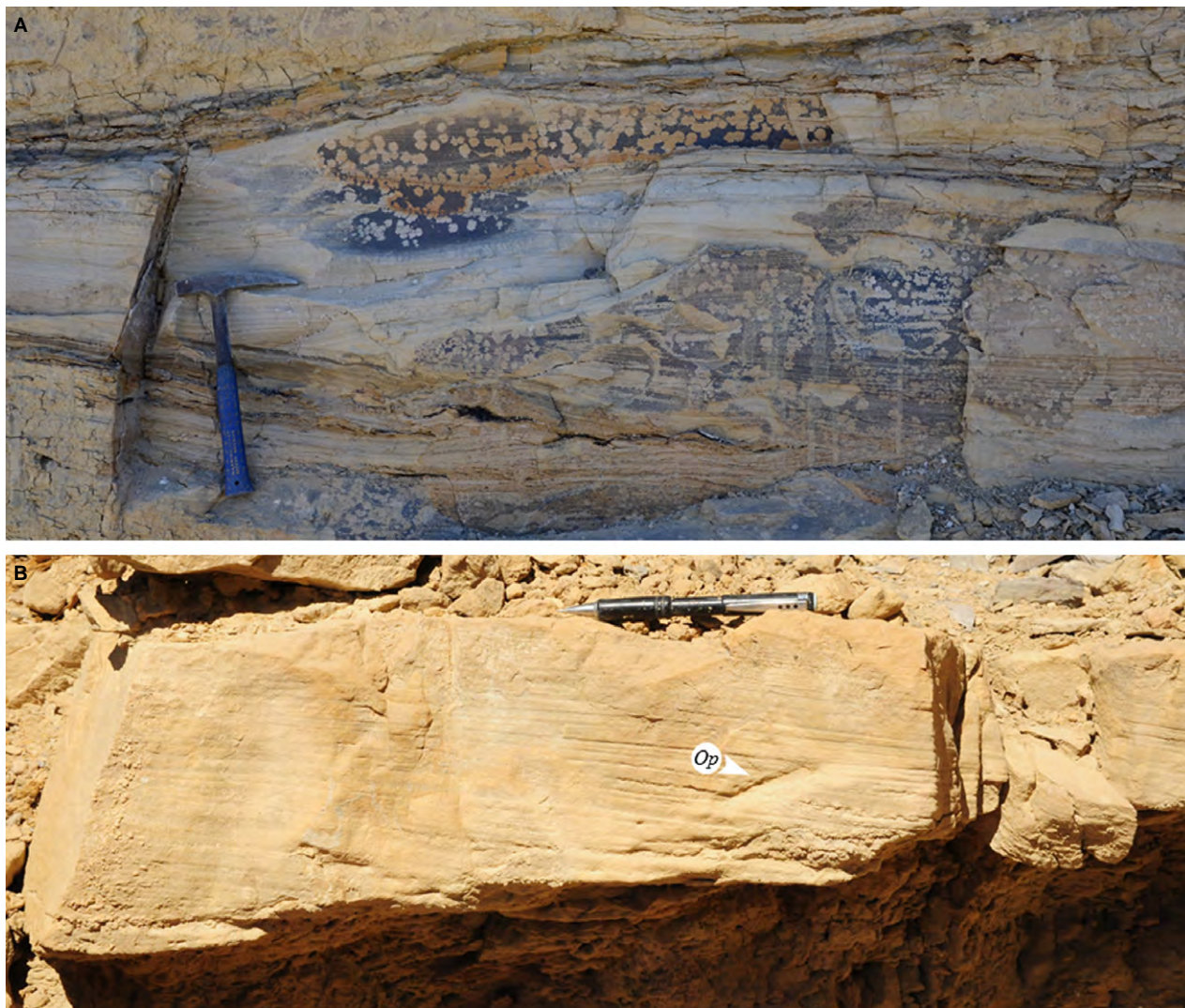
**Fig. 8.** Typical characteristics of fine-grained hyperpycnite deposits: (A) amalgamated normal grading and inverse to normal grading in muddy siltstone in measured section 7; (B) polished slab showing amalgamated normal grading and inverse to normal grading in muddy siltstone and silty mudstone in measured section 4, white arrows indicate burrows; (C) polished slab showing amalgamated inverse to normal grading in muddy siltstone from 2.35 to 2.45 m in measured section 3. The undulating dashed line indicates an erosional surface. Note that the inverse grading unit below the erosional surface on the left is totally eroded away to the right.

### FACIES PROPORTIONS AND LATERAL VARIABILITY

Table 1 presents details of all the sedimentary structures recorded in this study and the relative amount of sedimentary structures generated by fluvial-dominated and storm-dominated processes in each measured section (MS). Excluding the bioturbated intervals, the relative amount of fluvial and storm influence in each section can be calculated from the percentage of fluvial-generated and storm-generated sedimentary structures (combined-flow ripple lamination is assumed to reflect 50%

fluvial-influenced and 50% storm-influenced processes). The results in Table 1 indicate that the thin-bedded prodelta and distal delta-front facies within PS6–1 show a strong along-strike variation, with a wave-dominated environment (MS 1) in the northern area, passing abruptly into a fluvial-dominated, wave-influenced environment (MS 2 and MS 3) southward, then to an environment with varying degrees of fluvial and wave influence southward (MS 4 to MS 7), and back to a wave-dominated environment (MS 8 to MS 12) further to the south-east (see Fig. 2 for section locations and environment classification for each section in the bottom





**Fig. 9.** Typical characteristics of tempestite in outcrop. (A) Very fine-grained sandstone showing HCS capped by small wave-ripple laminations from 4.58 to 5.06 m in measured section 1. The hammer for scale is 28.5 cm in length. (B) Quasi-planar laminated very fine-grained sandstone bed in measured section 12 ('Op': Ophiomorpha). The pencil for scale is 13.5 cm in length.

row of Table 1). The facies successions characteristic of the thin-bedded facies in wave-dominated, fluvial-dominated and mixed fluvial-influenced and storm-influenced areas are described below. In order to avoid redundancy, only three end-member sections (MS 1, MS 2 and MS 4) are presented.

#### **Dominant wave/storm-influenced facies successions (MS 1 and MS 8 to MS 12)**

##### *Measured section 1: Wave-dominated, fluvial influenced*

In this section, the sandy facies have been adequately measured in previous studies (Li *et al.*,

2011, section 16 in fig. 4). The sandy facies are characterized by an upward coarsening succession showing wave-ripple lamination, quasi-planar lamination and dune-scale cross-bedding with archetypal *Cruziana* and *Skolithos* ichnofacies, which are interpreted to be the proximal lower shoreface and upper shoreface formed in a wave-dominated depositional environment (Li *et al.*, 2011). In the present study, the distal lower shoreface, which is prone to contain thin-bedded facies, has been measured in greater detail.

In measured section 1 (Fig. 10), 42% of the section is moderately to highly bioturbated and shows no distinct sedimentary structures



**Table 1.** All sedimentary structures recognized in this study and the relative percentages of different sedimentary structures generated by fluvial-dominated and wave-dominated processes present in each measured section: (a) no active depositional process occurs, also referred as ‘non-deposition’ in Fig. 5; (b) describes mudstone with silty laminations; (c) describes Bouma T<sub>B</sub> unit; (d) ratio between fluvial and wave influence; (e) based on the classification scheme proposed by Ainsworth *et al.* (2011) (an upper case letter refers to the dominant depositional process in the system, a lower case letter refers to the secondary process).

Depositional processes	Sedimentary Structures	MS 1	MS 2	MS 3	MS 4	MS 5	MS 6	MS 7	MS 8	MS 9	MS 10	MS 11	MS 12
Deposition pauses <sup>a</sup>	Bioturbated	41.67	33.20	15.54	29.55	31.11	56.56	22.74	53.64	18.24	20.80	33.73	45.92
Storm-dominated	Wave-ripple	22.26	0.00	4.42	29.86	23.19	21.69	20.86	21.21	40.05	24.70	47.85	39.52
	HCS	26.40	1.14	4.98	0.00	8.04	4.44	2.63	20.64	29.96	26.84	9.40	4.48
	Quasi-planar	7.44	0.00	0.00	0.00	0.00	1.69	1.48	0.00	0.00	0.00	0.00	3.31
Mixed fluvial-influenced and storm-influenced	Combined-flow ripple	0.53	0.00	3.19	5.14	0.00	0.00	2.27	2.10	0.21	2.49	1.17	0.00
Fluvial-dominated	Structureless	0.00	0.86	6.98	3.37	2.72	0.77	15.02	0.31	1.99	0.04	0.30	2.64
	Normal grading	0.20	0.95	11.68	9.02	3.57	3.65	7.47	0.16	3.20	4.26	2.13	0.81
	Inverse grading	0.00	0.00	4.81	1.36	0.24	0.00	0.96	0.00	0.16	0.43	0.00	0.00
	Starved ripple	0.06	0.77	0.91	1.54	6.98	2.08	1.42	0.41	0.29	2.57	1.01	0.00
	Laminated <sup>b</sup>	0.16	1.16	26.51	9.49	18.22	7.08	7.21	0.00	5.19	7.85	3.09	0.48
	Current ripple	0.89	24.56	19.79	1.62	5.49	1.59	14.16	1.09	0.16	2.76	0.44	0.91
	Planar lamination <sup>c</sup>	0.00	31.77	0.75	0.31	0.00	0.00	0.22	0.41	0.00	3.31	0.00	1.69
	Massive bedding	0.00	3.34	0.00	0.00	0.00	0.00	0.00	0.00	0.00	0.00	0.00	0.00
	Convolute bedding	0.00	0.00	0.00	8.25	0.00	0.00	0.09	0.00	0.00	0.00	0.00	0.00
NA	NA	0.40	2.23	0.45	0.49	0.43	0.45	3.46	0.03	0.56	3.95	0.89	0.25
F:W <sup>d</sup>		3.97	98.2	87.13	54.46	54.46	35.65	65.35	7.93	14.86	30.70	12.88	12.88
Classification <sup>e</sup>		Wf	Fw	Fw	Fw	Fw	Wf	Fw	Wf	Wf	Wf	Wf	Wf

(Table 1). About 56% of the beds contain quasi-planar lamination, HCS and wave-ripple lamination (Fig. 11). About 1.5% of the section is composed of normally graded muddy siltstone, laminated silty mudstone, and mudstone with starved ripple and current ripple laminations. The remaining 0.5% of beds show combined-flow ripple lamination. Figure 11C shows a typical interval from measured section 1. Sedimentary structures include combined-flow ripple lamination, current ripple lamination and wave-ripple lamination.

The BI log of the lower 3.13 m of section 1 shows a dominant uniform and high BI trend with some small intervals showing a non-uniform BI trend (Fig. 10). The BI log of the upper part of this section (above 3.13 m) is characterized by non-uniform, and uniform and low BI trends. The dominant strike direction measured from the crests of symmetrical wave ripples at this location is north-west/south-east (Fig. 12).

#### *Process interpretation*

More than 97% of the sedimentary structures and facies associations present in measured section 1 indicate deposition from storm-dominated oscillatory flows (Table 1). The presence of combined-flow ripple lamination, and the typical sequence of sedimentary structures shown in Fig. 11C, indicate deposition under the combined effects of both unidirectional flows (in this case, surge-type turbidity currents) and storm-dominated oscillatory flows (Myrow & Southard, 1991). However, sedimentary structures generated by purely unidirectional flows accounts for less than 3% of the whole section, suggesting that fluvial influence was rather small. The uniform and high BI trends in the lower part of the section indicate slower depositional rates, or low frequency (as indicated by some non-uniform BI trends) and low magnitude of depositional events, which probably results from dominant wave/storm influence (Gani *et al.*, 2008). Relatively lower BI in the upper part of the section, combined with a greater proportion of wave-formed sedimentary structures, indicates higher frequency and higher magnitude of storms, as the water depth becomes shallower upward. The northernmost area (measured section 1) of the strike-oriented Ferron Sandstone outcrop belt is thus interpreted to be dominated by wave processes with only a minor amount of fluvial influence.

Similar to section 1, the thin-bedded facies measured in sections 8 to 12 are characterized by more than 70% storm-generated sedimentary

structures (Table 1). The greater abundance of bioturbated beds and dominant uniform BI trend in these sections also indicate slower rates of deposition, which may be linked to a more wave-dominated regime (MacEachern *et al.*, 2005). Some intervals of non-uniform BI trends in these sections indicate variable frequency and magnitude of depositional events, including surge-type turbidity currents, hyperpycnal flows and storm surges. The relatively small proportion of sedimentary structures generated by unidirectional-current-dominated flows indicates that the fluvial influence at these localities is subordinate.

### **Dominant fluvial-influenced facies successions (MS 2 and MS 3)**

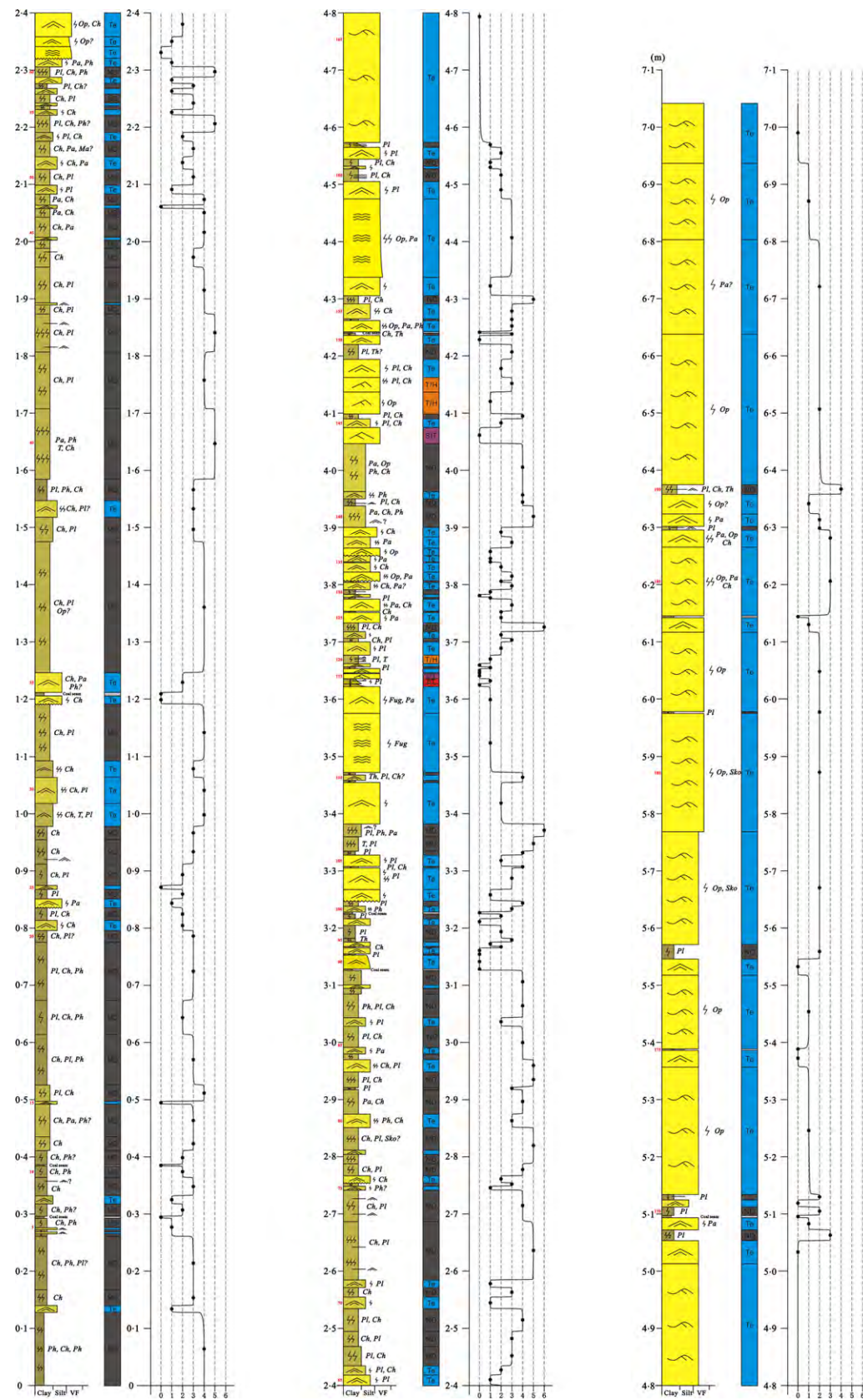
#### *Measured section 2: Fluvial-dominated, wave influenced*

Measured section 2 (Fig. 13) consists of *ca* 33% bioturbated beds showing no distinct sedimentary structures. More than half of the beds show sedimentary structures, such as massive bedding, planar lamination and current ripple lamination (Table 1). Less than 5% of this section is composed of laminated mudstone, normally graded muddy siltstone and structureless mudstone (Figs 4, 7 and 8C). Hummocky cross-stratification (Fig. 14) only accounts for 1% of the section. Common successions of sedimentary structures and grading patterns present in this section are shown in Fig. 15.

The BI log for section 2 shows a bi-modal pattern. The lower 2.4 m of the BI log (Fig. 13) is characterized by a non-uniform BI trend and the upper part (above 2.4 m) is dominated by a uniform and low BI pattern. Palaeocurrent data measured from current ripples and starved ripples in sections 2 and 3 are dominantly directed towards the north-east and east (Fig. 12). The dominant strike direction of wave-ripple crests in these locations is north-east/south-west (Fig. 12).

#### *Process interpretation*

Within section 2, more than 98% of the event beds contain sedimentary structures which are indicative of deposition from fluvial-dominant processes (Table 1), including surge-type turbidity currents and hyperpycnal flows (Figs 4 and 7). Less than 2% of the sedimentary structures indicate deposition under strong oscillatory flows and the rare HCS indicates a minor component of storm-wave reworking. However, by combining the sedimentary structures and grading patterns of the beds below and above the HCS beds, the



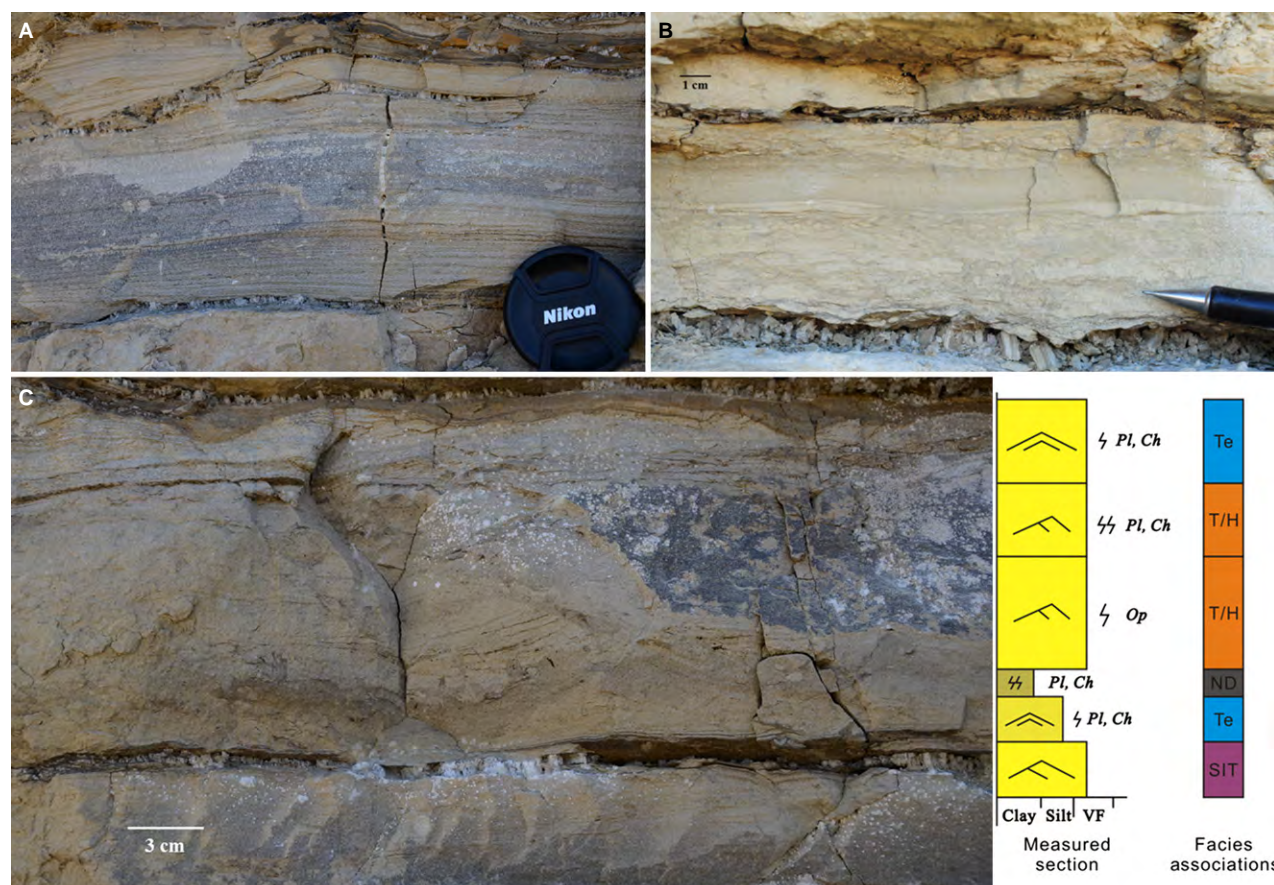


**Fig. 10.** Measured section 1, with interpreted facies-associations and BI log, showing a typical wave-dominated succession. See Fig. 5 for facies keys and Fig. 2 for location of the section. Small red numbers on the left of the thickness axis indicate the number of the bed recorded in the section.

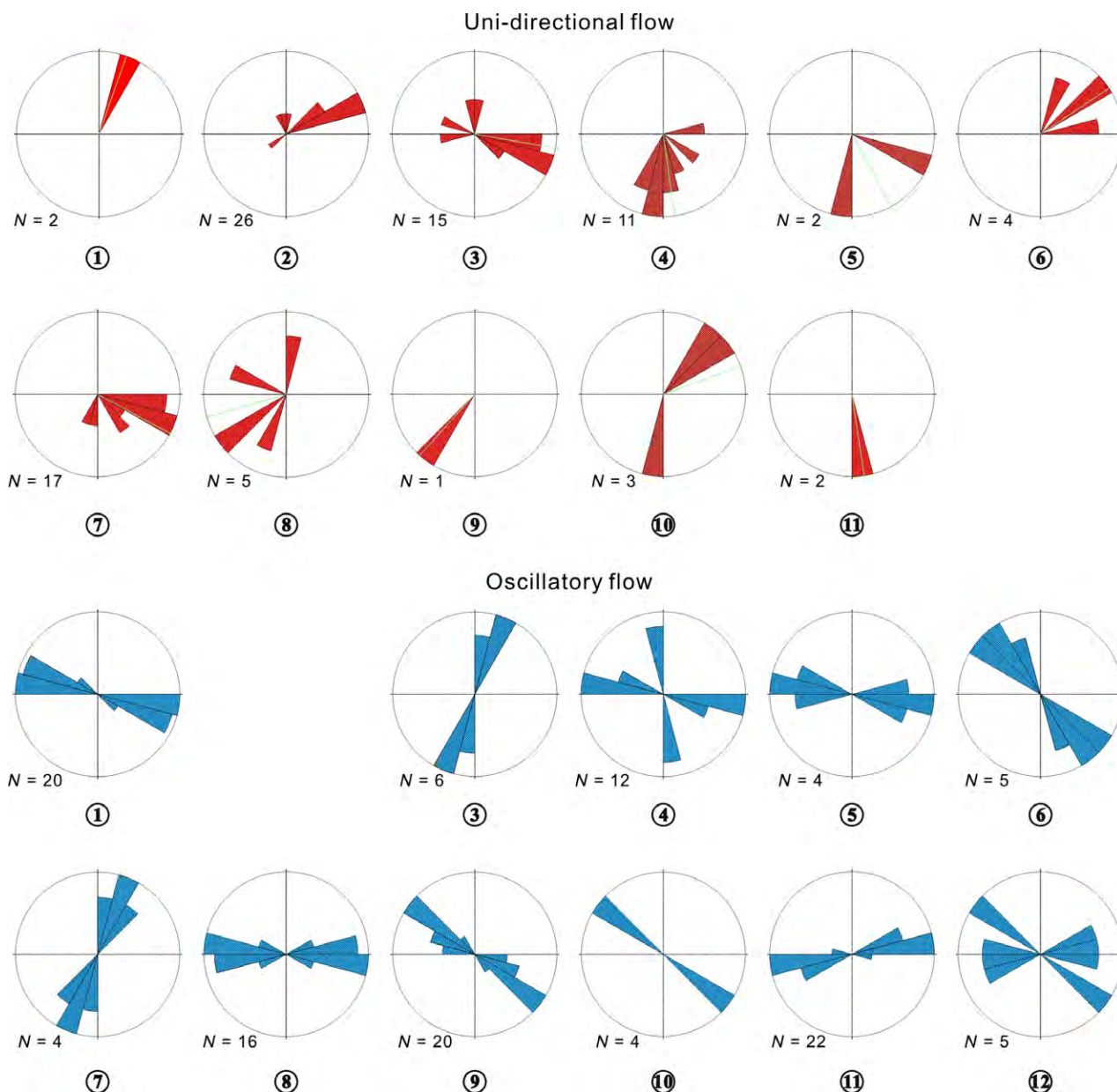
facies association shows an overall inverse to normal grading pattern (Fig. 14). The particular grading pattern and sequence of sedimentary structures indicates deposition from the combined effects of storm surges that were probably linked and would have been responsible for generating some of the hyperpycnal flows.

Normally graded bedding and partial Bouma sequences, indicating deposition from surge-type turbidity currents, are common (Fig. 15, draw-

ings 1 to 3). Inverse to normal graded beds and wax-wane stratification sequences indicate deposition from sustained hyperpycnal flows (Fig. 15, drawings 5 to 8). The non-uniform BI indicates variable frequency and magnitude of depositional events (Gani *et al.*, 2008) in the lower section, whereas the uniformly low BI in the upper part of the section indicates a persistently stressful environment (MacEachern *et al.*, 2005) resulting from salinity and turbidity variations due to high



**Fig. 11.** Thin-bedded facies generated by dominant wave/storm influence. (A) Very fine-grained sandstone showing quasi-planar lamination capped by small wave-ripple laminations from 3.47 to 3.62 m in measured section 1. The camera lens cap for scale is 6.5 cm in diameter. (B) Outcrop showing lam-scam bedding which is characterized by wave-ripple lamination overlain by highly bioturbated silty mudstone, from measured section 12. Note the remnant wave-ripple lamination (right above the pencil tip) within the highly bioturbated silty mudstone. (C) Outcrop (left) from 4.04 to 4.19 m in measured section 1 with the correlated measured section and interpreted facies associations. From the bottom to the top, the sedimentary structures present in each bed include combined-flow ripple laminations, wave-ripple laminations, NA (bioturbated), current ripple laminations and wave-ripple laminations. See Fig. 5 for facies key.



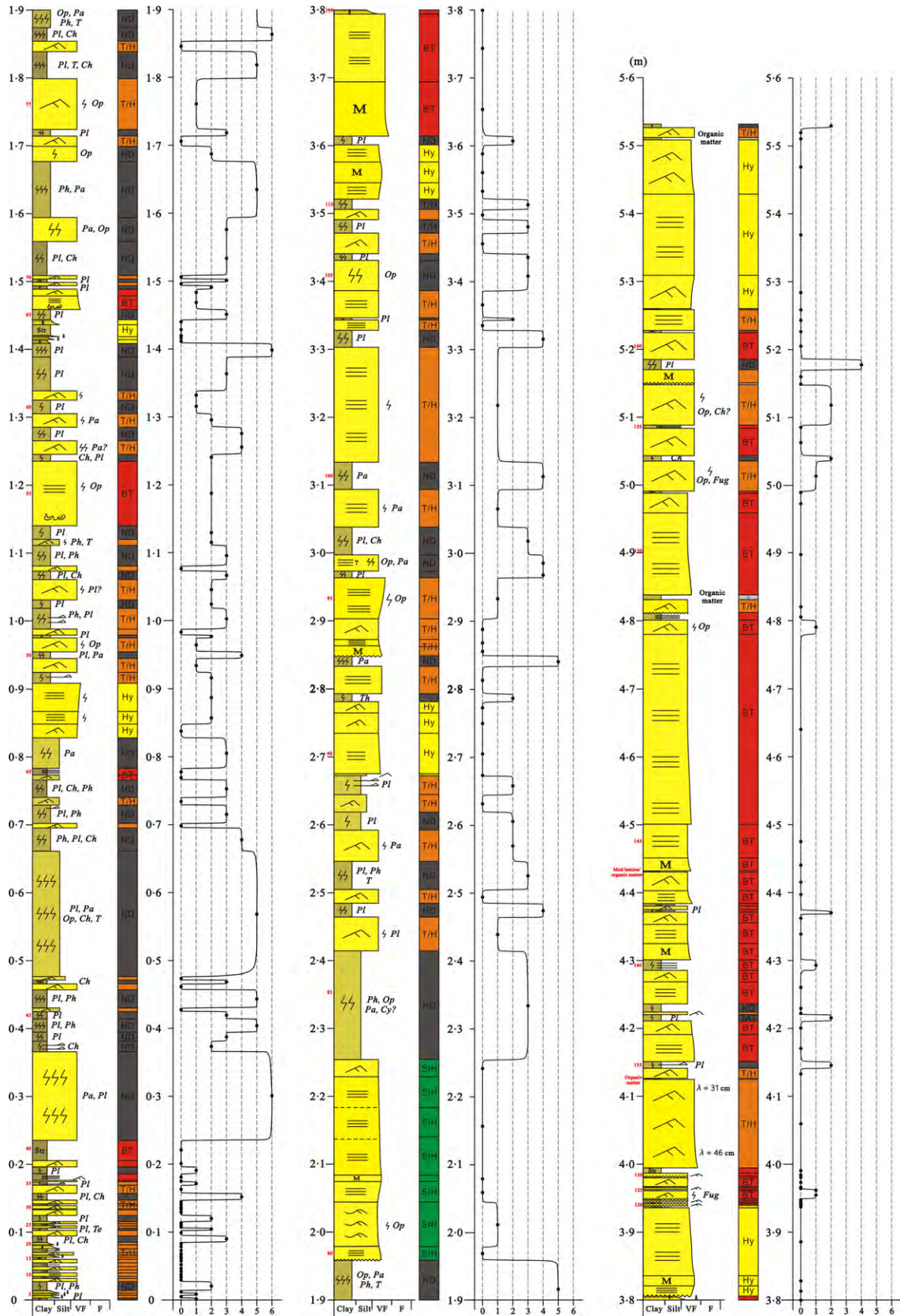
**Fig. 12.** Rose diagrams showing palaeocurrent directions at each measured section. Directions of unidirectional flows are measured from current ripples and combined ripples. Directions of oscillatory flows are measured from crests of wave ripples and combined ripples. See Fig. 2 for locations of sections.

frequency and high magnitude depositional events of surge-type turbidity currents and hyperpycnal flows. Measured section 2 is interpreted to be river dominated with only minor storm influence.

Measured section 3 also contains a major proportion (87%) of sedimentary structures typical of deposition from unidirectional flows (Table 1). The uniform and low BI in the lower part of section 3 indicates a persistently stressful

**Fig. 13.** Measured section 2, with interpreted-facies associations and BI log, showing a typical river-dominated succession. See Fig. 8 for facies keys and Fig. 2 for location of the section. Small red numbers on the left of the thickness axis indicate the number of the bed measured in this section.

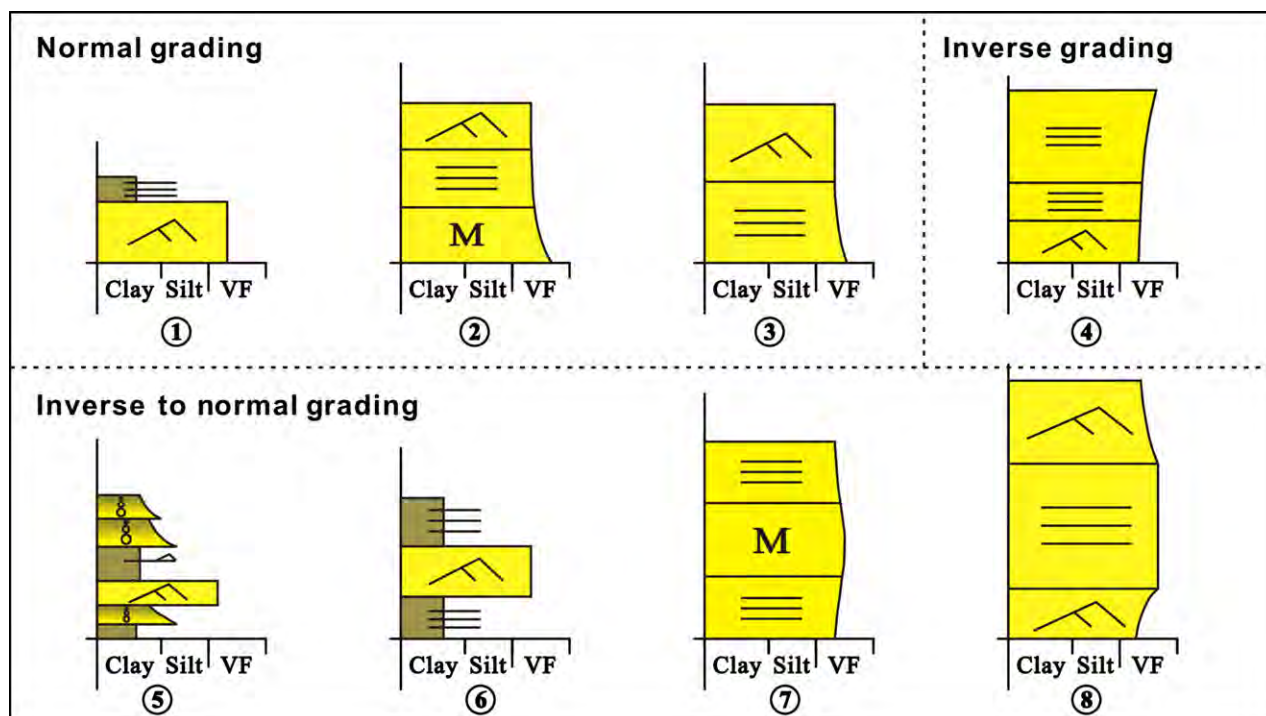






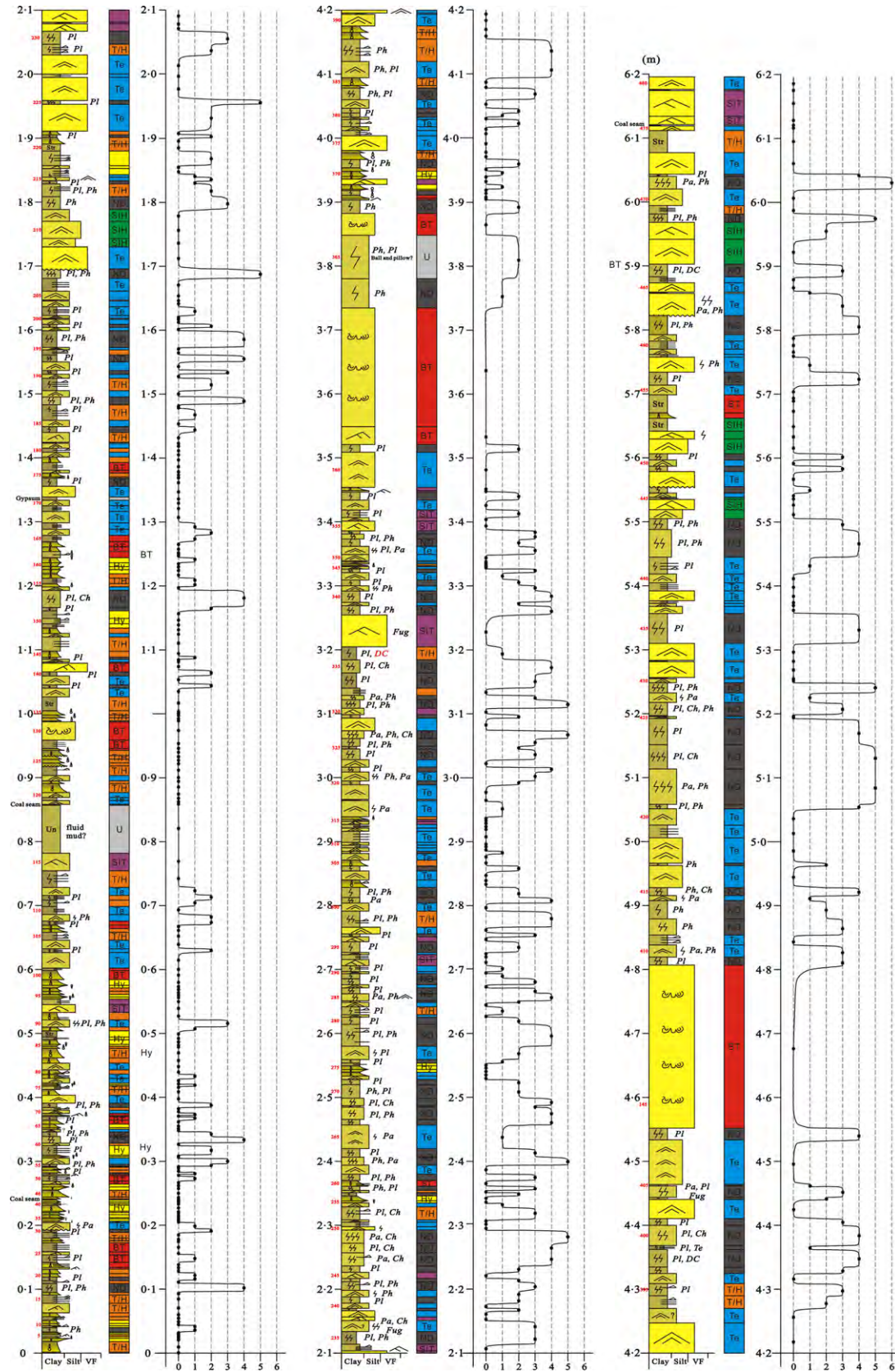


**Fig. 14.** Outcrop (left) from 2.07 to 2.47 m in measured section 2 with the correlated measured section, interpreted facies associations, and BI log. From the bottom to the top, sedimentary structures pass from planar lamination, well-preserved HCS, then inversely grade to planar laminations, massive bedding, then overlain by normally graded beds with planar laminations and current ripple laminations. See Fig. 5 for facies key.



**Fig. 15.** Schematic drawings of the common grading sequences among event beds presented in measured section 2. Total thicknesses range from several millimetres to decimetres. See Fig. 5 for facies key.

**Fig. 16.** Measured section 4, with interpreted facies-associations and BI log, showing a typical wave-influenced and fluvial-influenced succession. See Fig. 5 for facies key and Fig. 2 for location of the section.





environment (MacEachern *et al.*, 2005) caused by high frequency and high magnitude depositional events of surge-type turbidity currents and hyperpycnal flows. The proportion of sedimentary structures generated by storm processes, such as HCS, wave-ripple lamination and combined-flow lamination, increases upward. Both the BI trend and sedimentary structures indicate that the upper part of this section is deposited from turbidity-current and storm-surge events of variable frequency and magnitude. Therefore, measured section 3 is interpreted to be deposited under dominant fluvial influence with a higher amount of storm influence compared with section 2.

### Mixed fluvial and wave/storm-influenced facies successions (MS 4 to MS 7)

#### *Measured section 4: Fluvial-dominated, wave influenced*

In measured section 4 (Fig. 16), *ca* 30% of the section is bioturbated and *ca* 30% of the beds contain wave-ripple laminations (Table 1). Ten per cent of the beds show sedimentary structures, such as planar lamination, current ripple lamination and convolute bedding. Twenty-five percent of the section is composed primarily of fine-grained facies, including laminated mudstone, normally graded muddy siltstone, inversely graded muddy siltstone (Fig. 8B), mudstone with starved ripple laminations and structureless mudstone. The remaining 5% of beds show combined-flow ripple lamination.

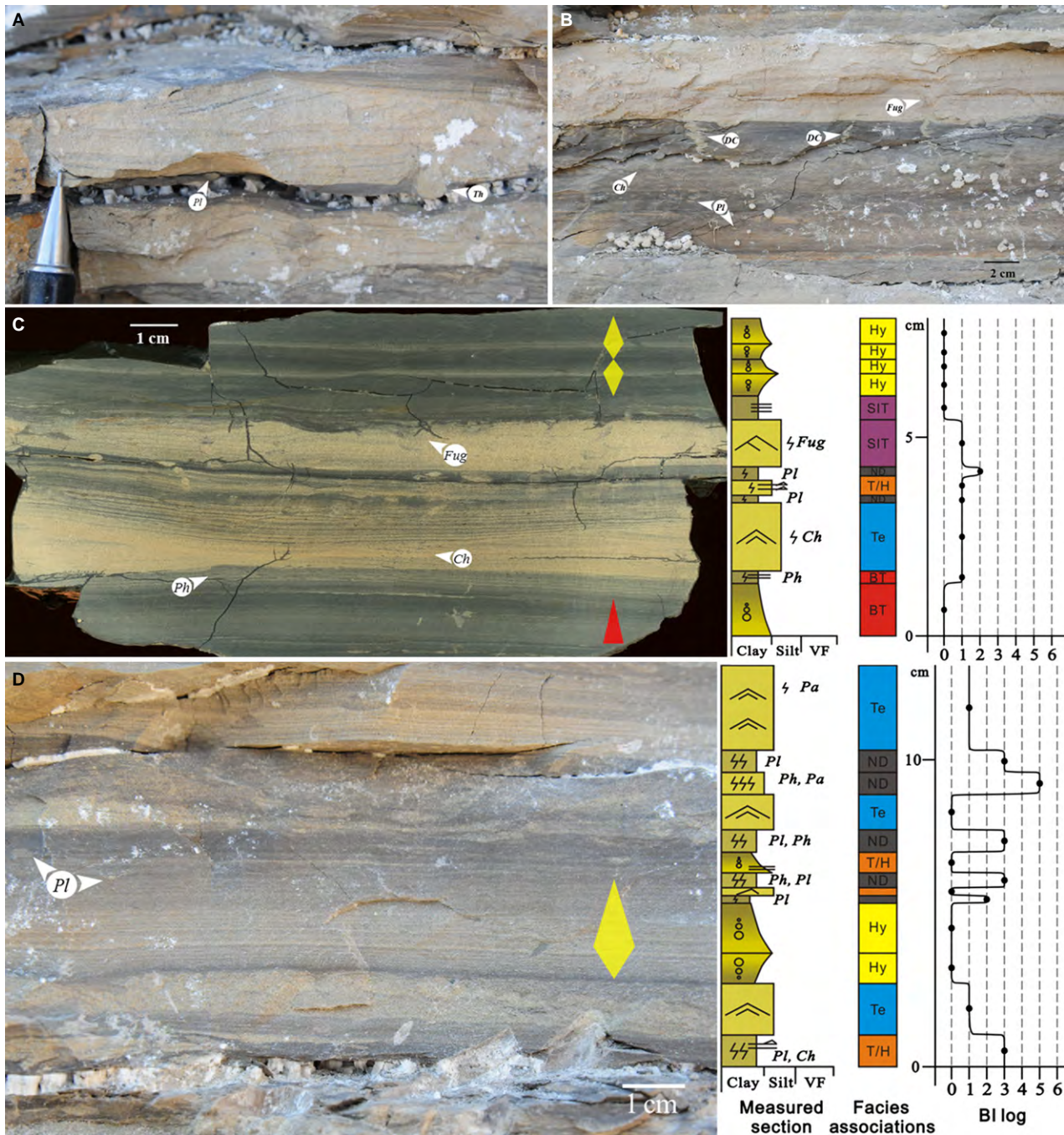
Figure 17A shows a bed of very fine sandstone containing well-developed combined-flow ripple laminations, which are characterized by rounded crests, a nearly symmetrical shape and unimodally dipping foresets. Figure 17B shows a bed of very fine-grained sandstone containing *Fugichnia* overlying slightly bioturbated silty mudstone with dewatering cracks. Figure 17C shows a polished rock sample showing a typical interval from measured section 4. From the bottom to the top, distinct facies present in this interval include normally graded silty mudstone overlain by mudstone with silty laminations, wave-ripple lamination, combined-flow ripple lamination and two amalgamated inversely to normally graded silty mudstones. Similarly, typical facies present in Fig. 17D include mudstone with silty laminations (starved ripple), muddy siltstone showing inverse to normal grading, moderately bioturbated silty mudstone and muddy siltstone containing wave-ripple laminations.

The BI log for section 4 is dominated by a non-uniform BI trend (Fig. 16). Palaeocurrent data recorded from sections 4 to 7 also indicate that the dominant direction of unidirectional flows is to the north-east/east (Fig. 12). In this area, the dominant strike direction of wave-ripple crests is north-west/south-east (Fig. 12).

#### *Process interpretation*

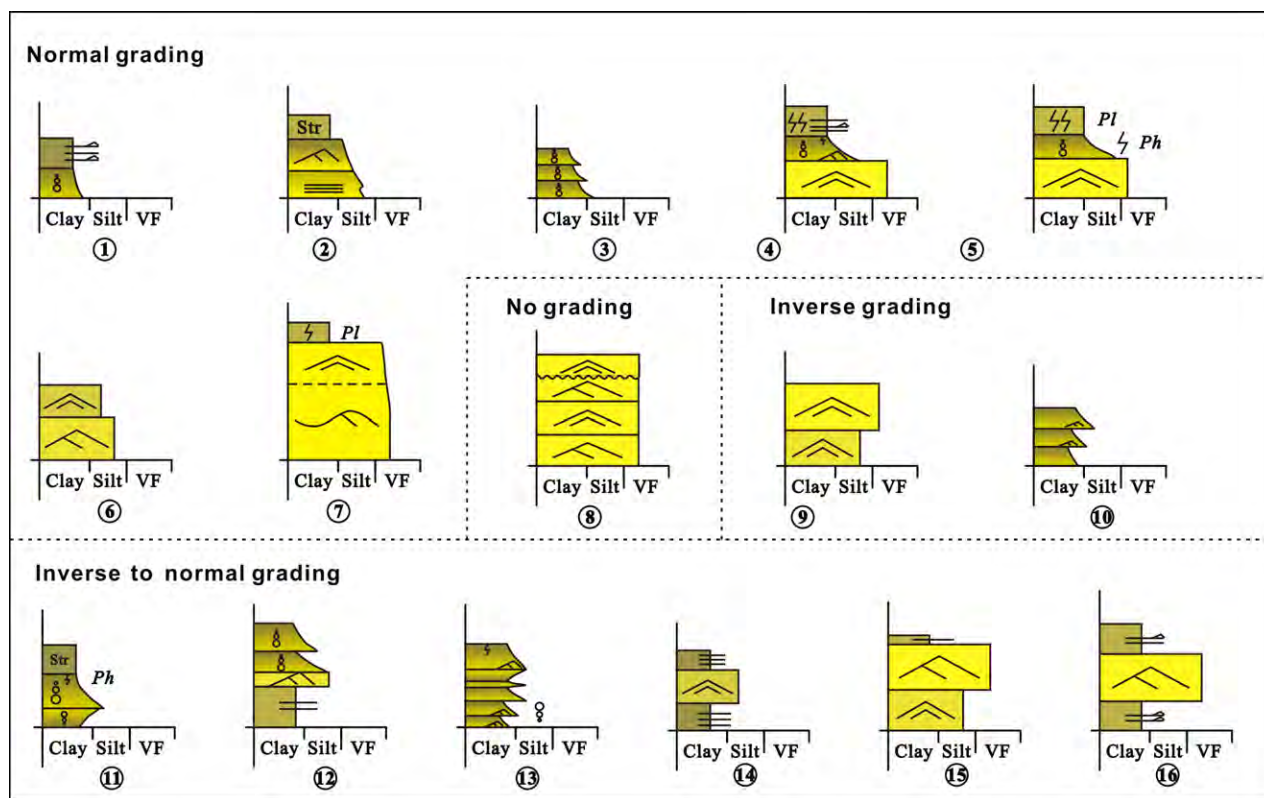
The presence of combined-flow ripple lamination and specific trace fossils in measured section 4 indicate deposition under combined-flow conditions, and also indicate the influence of both hyperpycnal flows and storm-dominated oscillatory flows. The trace-fossil escape structure (*Fugichnia*) is generally associated with sporadic depositional events, such as turbidity currents or storm surges (MacEachern *et al.*, 2005). The presence of dewatering cracks may indicate salinity fluctuation caused by strong freshwater input (fluvial influence). Both the sedimentary structures and the non-uniform BI trend indicate variable frequency and magnitude of depositional events of surge-type turbidity currents, hyperpycnal flows and storm surges. The relative proportions of facies indicate an equally mixed fluvial-wave influenced setting.

The depositional environment in the area from measured sections 4 to 7 is interpreted to be a mixed-process environment, which is exposed to both strong fluvial and wave influence. The relative amount of fluvial and storm influence varies from measured sections 5 to 7 (Table 1), which could be due to palaeogeography or proximity to a distributary channel system, and will be discussed in more detail in the *Along-strike variation in depositional processes* section below. Common sequences of sedimentary structures and grading patterns among event beds also indicate the combined effects of turbidity currents and storm surges (Fig. 18). Normally graded successions with partial Bouma sequences strongly indicate deposition from surge-type turbidity currents (Fig. 18, logs 1 to 3). Overall inverse to normally graded successions probably indicate deposition from hyperpycnal flows (Fig. 18, logs 11 to 13). Normally graded successions showing sedimentary structures generated by storm-dominated oscillatory flows are interpreted as tempestites (Fig. 18, log 7). Other normally graded, inverse to normally graded, inversely graded and non-graded beds consisting of sedimentary structures that are indicative of deposition from both unidirectional and oscillatory flows (Fig. 18, logs 4 and 5, 8 and 9, and 14 to 16) suggest frequent



**Fig. 17.** Thin-bedded facies generated by mixed fluvial and storm influence. (A) Well-developed combined ripple lamination at 3.10 m in measured section 4. (B) Moderately to slightly bioturbated silty mudstone overlain by very fine sandstone showing combined-flow ripple laminations, from 3.16 to 3.25 m in measured section 4. (C) Polished rock sample (left) from 0.58 to 0.67 m in measured section 4 with the correlated measured section, interpreted facies associations and BI log. (D) Outcrop (left) from 2.32 to 2.45 m in measured section 4 with the correlated measured section, interpreted facies associations and BI log. See Fig. 5 for facies keys. Trace-fossil abbreviations include: Chondrites (*Ch*), Planolites (*Pl*), Thalassinoides (*Th*) and trace-fossil escape structure (*Fug*: Fugichnia). Dewatering cracks (*DC*) occur locally.





**Fig. 18.** Schematic drawings of the common grading sequences among event beds presented in measured sections 4 to 7. The beds show a wide variety of grading patterns: normal grading (1 to 7), no grading (8), inverse grading (9 and 10) and inverse to normal grading (11 to 16). Total thicknesses range from several millimetres to decimetres. See Fig. 5 for facies key.

interactions between successive turbidity currents (i.e. surge-type turbidity currents and hyperpycnal flows) and storm surges.

In all four measured sections (sections 4 to 7), the relative amount of sedimentary structures generated by storm-dominated oscillatory flows increases towards the top of each section, which indicates that the frequency of storm events increases as the water depth becomes shallower. The dominant non-uniform BI trend for all four sections also indicates variable frequency and magnitude of depositional events (i.e. surge-type turbidity currents, hyperpycnal flows and storm surges).

## DISCUSSION

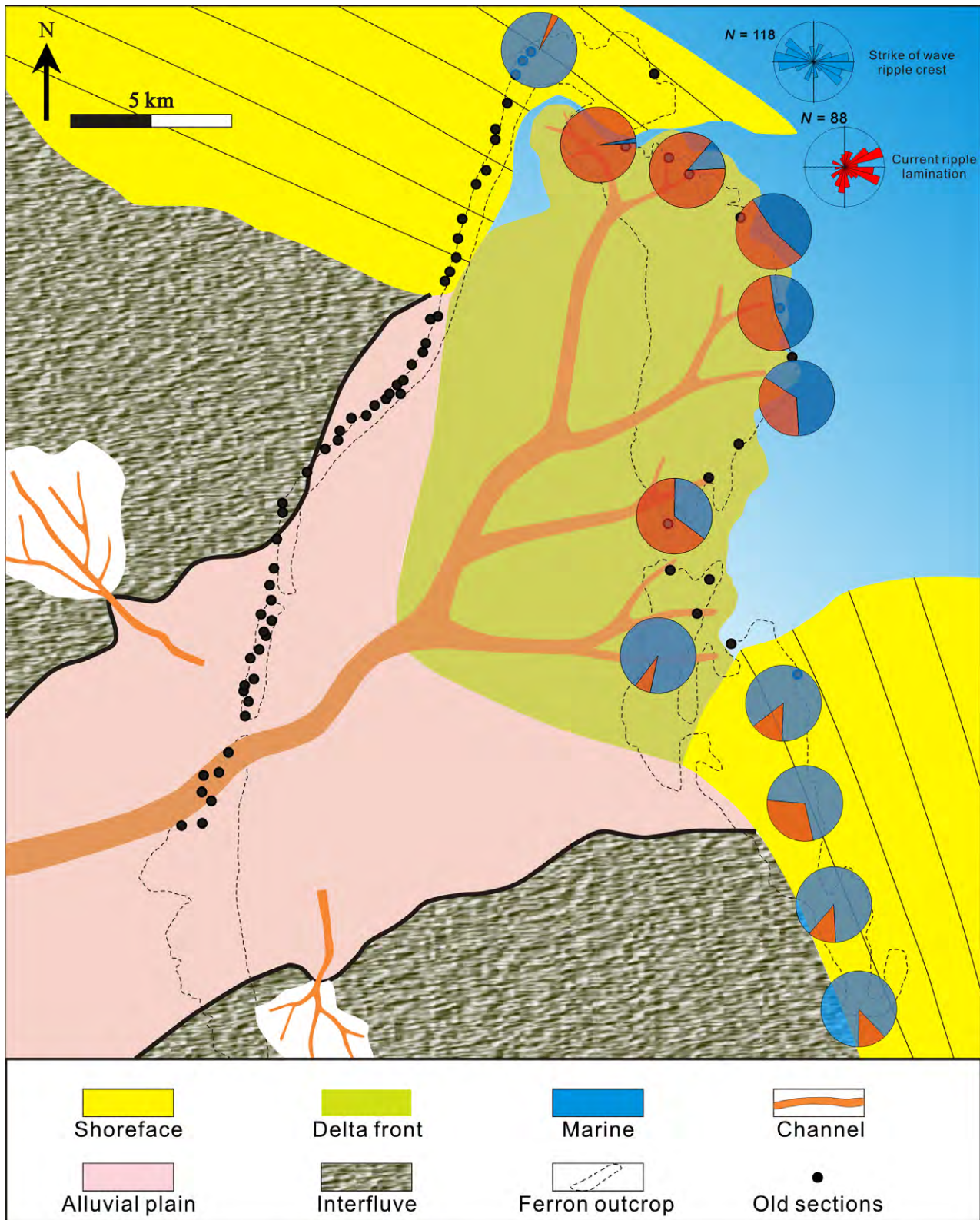
### Along-strike variation in depositional processes

Based on the different types of sedimentary structures, and the relative amount of sedimen-

tary structures and facies associations present in the 12 measured sections, the thin-bedded prodelta and distal delta-front facies of PS6–1 show a strong along-strike variation in dominant depositional processes. This variation is interpreted to be caused by the interactions between fluvial-dominated and storm-dominated processes along depositional strike. The complex lateral variations in the dominant depositional process shown in this study indicate that PS6–1 is a mixed-influenced delta (Fig. 19).

Measured section 1 is dominated by wave/storm influence. The dominant direction of oscillatory storm surges, as indicated by the strike direction of wave-ripple crests in this location, is north-east/south-west (Fig. 12); this corresponds to the southerly direction of net sediment transport along the western margin of the seaway, as suggested by regional palaeoenvironmental reconstructions (Ericksen & Slingerland, 1990; Slingerland & Keen, 1999).

The muddy facies in this section are characterized by a moderate to high bioturbation index,



**Fig. 19.** Schematic drawing of the palaeogeographic reconstruction of parasequence 6 (based on Li *et al.*, 2011; Ahmed *et al.*, 2014; and results from this study). The pie charts show the relative amount of fluvial-dominated (red) and storm-dominated (blue) depositional processes at different localities of measured sections (indicated by the centre of the pie chart) of thin-bedded facies in this study. All the palaeocurrent data from all 12 sections are combined and shown at the upper right corner.



which indicates longer ambient periods between successive storm events. The thick sandy shoreface in the northern area is interpreted to have formed a barrier, which protected the bay area to the south from strong wave influence.

Measured sections 2 and 3 are located in a fluvial-dominated environment with only minor storm influence. Previous studies (Li, 2012; Ahmed *et al.*, 2014) show a predominance of distributary channels in this area, which also suggests fluvial dominance. As shown in Fig. 19, these two sections are located in the bay area.

Palaeocurrent data measured from current ripples and starved ripples from these two sections indicate that the dominant direction of unidirectional flows is to the north-east and east (Fig. 12), which is consistent with the progradation direction of the ancient delta system. Measurements from the crests of wave ripples in section 3 indicate that the dominant directions of oscillatory storm surges are north-west/south-east (Fig. 12), which suggest that severe storms occasionally passed around the shoreface barrier and intruded into this bayhead area (Fig. 19). This phenomenon also explains the higher proportion of storm-generated sedimentary structures in section 3 compared with section 2, because section 3 is located further out in the embayment (Fig. 19).

Measured sections 4 to 7 are located in a mixed environment with varying amounts of fluvial and wave influence. The relatively strong fluvial influence in these two sections can be explained by the proximity to a distributary channel system (Li, 2012). However, the relative amount of storm influence in sections 4 and 5 increases significantly from *ca* 10% to *ca* 50% compared to sections 2 and 3, which indicates that the barrier effects of the shoreface in the north are less significant in this area (Fig. 19). Further south of the distributary channel systems, measured section 6 shows a dominance of

wave over river influence. Palaeocurrent data of unidirectional flows recorded from sections 4 to 7 also indicate a dominant north-eastward to eastward transport direction (Fig. 12). The subordinate southward direction indicates that the sediment load carried by the distributary channel systems was deflected southward by strong longshore currents, similar to those documented by Fielding (2010) in outcrops further south, which is also consistent with previous numerical modelling of circulation in the seaway (Ericksen & Slingerland, 1990; Slingerland & Keen, 1999). The orientation of wave-ripple crests indicates that the dominant directions of oscillatory storm surges in this area are north-east/south-west (Fig. 12), which also suggests that the barrier effect of the shoreface was negligible in this area.

Measured sections 8 to 12 are located in a storm-wave dominated area with only minor river influence, reflecting that they are further away from the previously mapped distributary channel systems. Palaeocurrent data measured from these five sections suggest a dominant southward flow direction (Fig. 12), which is due to the southward deflection of the river plumes by strong longshore currents. The dominant oscillatory directions of storm surges are also oriented north-east/south-west (Fig. 12), which again indicates an open environment exposed to direct storm influence.

In summary, PS6–1 shows strong along-strike variation in fluvial versus fair-weather and storm-wave influence. By combining the results from all 12 sections, the relative amounts of fluvial and wave influence for the whole delta system are 39% and 61%, respectively. Integrated with the along-strike variation, PS6–1 is interpreted to be a storm-dominated symmetrical delta with a large bayhead system. However, results from this study indicate that force-fitting this delta into any end-member type, or

**Table 2.** Comparison of the relative amount of fluvial and wave influence derived from sandy facies (Li *et al.*, 2011), and the thin-bedded facies.

%	Depositional process	MS 1	MS 2	MS 3	MS 5	MS 6	MS 7
Li <i>et al.</i> (2011)	Fluvial	0	100	100	50	50	100
	Wave	100	0	0	50	50	0
This study	Fluvial	3	98	87	54	35	65
	Wave	97	8	13	46	65	35

even any area of the tripartite delta classification (Galloway, 1975; Ainsworth *et al.*, 2011), may not fully reveal the complex along-strike variation reflected in the internal thin-bedded facies. Important factors that control the dominant depositional processes within this delta system include the proximity to distributary channels (fluvial influence), strong storm influence in the Western Interior Seaway and local palaeogeography (barrier from marine influence). The persistence of the river-dominated bayhead delta may be associated with the fact that feeding rivers were entrenched in an incised valley (Zhu *et al.*, 2012; Ahmed *et al.*, 2014).

### Sandy facies versus muddy facies

The question of whether the relative amounts of river and wave influence calculated from the thin bedded facies are consistent with previous results from analysis of primarily sandy facies (Li *et al.*, 2011) are now addressed. The sandy facies measured by Li *et al.* (2011) include: proximal delta front, distributary channel and mouth-bar facies in the fluvial-dominated environments; upper shoreface and foreshore facies in the fair-weather wave-dominated environments; and mixed storm-wave-reworked delta-front facies. By calculating the relative percentage of different facies generated from river and wave processes, the relative amount of river and wave influence can be determined in a similar way. Six sections measured in this study are located either at the same positions or very close to sections measured by Li *et al.* (2011). A comparison between the relative amount of river and wave influence derived from the sandy facies and the thin-bedded facies is presented in Table 2.

As shown in Table 2, results derived from the sandy facies and the thin-bedded facies are consistent in the areas which are dominated by one type of depositional process (for example, wave-dominated section 1 and fluvial-dominated sections 2 and 3). However, in mixed-influenced environments, it is difficult to exclusively use the sandy facies to determine the relative amount of river-dominated and wave-dominated depositional processes (sections 5 and 6). In some sections, the sandy facies cannot resolve the relative amounts of different depositional processes (section 7). Possible reasons include: (i) the study conducted by Li *et al.* (2011) was aimed at regional stratigraphy rather than evalu-

ation of the complex mixed-process delta system within one single parasequence; and (ii) sections measured by Li *et al.* (2011) focused more on the facies architecture of elements in each parasequence, rather than the bed-scale sedimentary structures generated by different depositional processes, which inherently neglects the combined effects of various depositional processes and thus makes it almost impossible to calculate the exact percentage of different depositional processes. For example, in measured sections 5 and 6, Li *et al.* (2011) grouped all of the sandy facies above the thin-bedded prodelta facies as wave/storm-reworked delta-front facies. However, because these sections are measured at a coarser scale, the exact degree of wave/storm reworking cannot be determined (Table 2). In measured section 7, the sandy facies directly above the thin-bedded facies measured in this study is a 2.5 m thick medium-grained sandstone containing dune-scale cross-bedding, which is interpreted to be the distributary channel facies (Li *et al.*, 2011). If only accounting for the sandy facies, measured section 7 would be 100% river dominated. Obviously, this interpretation significantly underestimates the 35% wave influence (Table 2), as indicated by the wave-ripple lamination and HCS present in the event beds within the thin-bedded facies.

To conclude, the relative amounts of different depositional processes calculated from the thin-bedded facies and the sandy facies above are consistent in the areas dominated by one type of environment. In a mixed-process environment, only considering the sandy facies may not be sufficient to reveal the relative proportion of different depositional processes. The complex interactions between different depositional processes are more likely to be recorded by the thin-bedded prodelta facies and the heterolithic distal delta-front facies.

### Significance of hypopycnal flows

Based on the analysis of sediment and water budgets of 150 rivers that discharge into the sea, Mulder & Syvitski (1995) concluded that small to medium-sized rivers are more likely to produce hypopycnal flows at least once every 100 years during flood periods. The critical sediment concentration needed to generate hypopycnal plumes is proposed to be 35 to 45 kg m<sup>-3</sup> (Mulder & Syvitski, 1995). However, this limit may decrease significantly due to sediment-driven convection (Parsons *et al.*, 2001), during cata-



Facies associations	MS 2	MS 3	MS 4	MS 5	MS 6	MS 7
Bouma-type turbidite	34.98	22.49	17.45	10.76	2.99	16.12
Hyperpycnite	18.27	13.46	6.34	4.94	0.00	5.13
Bouma-type turbidite/hyperpycnite	38.88	48.53	19.50	43.73	32.25	35.76
Tempestite	0.00	12.10	44.95	40.57	64.76	39.25
Storm-influenced turbidite	0.00	3.42	6.93	0.00	0.00	3.74
Storm-influenced hyperpycnite	7.86	0.00	4.83	0.00	0.00	0.00

**Table 3.** Relative proportion of facies associations generated by different depositional processes in measured sections 2 to 7.

strophic extreme events (Mulder *et al.*, 2003) and due to other effects, such as density stratification and mixing in an estuary and lowering of salinity in the immediate offshore area of a river mouth (Felix *et al.*, 2006; Bhattacharya & MacEachern, 2009) which, in turn, suggests that many smaller rivers could commonly generate hyperpycnal flows in the shallow marine environment, and that their deposits should have more importance in the geological record than previously recognized (Mulder & Chapron, 2011).

Estimations of the palaeo-discharge of the ancient Ferron rivers indicate that those rivers could frequently produce hyperpycnal flows (Bhattacharya & MacEachern, 2009). The proximity to the Sevier orogenic belt also promoted the Ferron rivers to achieve hyperpycnal states. Another important cause of hyperpycnal flows in this ancient delta system is the sustained river-flooding linked to severe storm events, or the so-called ‘oceanic floods’ proposed by Wheatcroft (2000). Different from seasonal floods that characterize moderate to large rivers, oceanic floods are likely to affect small rivers, in which elevated river discharge is caused by storm events over short time periods (Wheatcroft, 2000). At the locality of measured section 3 in this study, the sandy delta-front facies contain beds showing aggrading symmetrical wave ripples that transition to climbing unidirectional-current ripples (Garza, 2010). This typical facies association indicates rapid deposition caused by a river flood event in the presence of a storm. The importance of storm-induced flood events is also supported by results in this study. For example, Fig. 14 shows a basal tempestite directly overlain by a hyperpycnite. Figure 17C and D show sedimentary structures generated by storm-dominated oscillatory flows (i.e. wave-ripple lamination) that pass upward to sedimentary

structures (i.e. inverse to normal grading) generated by hyperpycnal flows. When the storm begins to wane, the influence of river-flooding becomes dominant, therefore resulting in facies associations in which river-fed hyperpycnites directly overlie storm-induced tempestites.

In this study, hyperpycnites are recognized in measured sections 2 to 7, which are located in environments under strong to dominant fluvial influence. However, the question remains as to how great a proportion of hyperpycnites is present in the depositional record of a fluvial-dominated delta system?

In order to evaluate the relative importance of hyperpycnal flows among all depositional processes within this ancient delta system, the proportion of facies associations in which the sedimentary structures are disrupted by burrows or where simply no sedimentary structures can be determined are firstly excluded. Then, based on the typical sequence of sedimentary structures and grain-size variations, facies associations generated by different depositional processes can be interpreted and calculated within each measured section. As shown in Table 3, when considering all possible depositional processes, the relative proportion of hyperpycnites that can be recognized with confidence in each section is actually rather small. For example, in measured sections 2 and 3, which are dominated by river influence, less than 20% of the event beds are confidently recognized as hyperpycnites. In measured sections 4 to 7, less than 10% of the event beds are likely to have been generated by hyperpycnal flows. In each of these six sections, the proportion of Bouma-type turbidites is about twice the proportion of hyperpycnites. One possible explanation for this discrepancy is that a surge-type turbidity current is a more

important depositional process compared with hyperpycnal flow in a river-dominated delta. This explanation seems to contradict the statement that hyperpycnal flows are commonly generated in ancient Ferron rivers (Bhattacharya & MacEachern, 2009). However, the relative proportion of hyperpycnal flows in each section may be underestimated in the present study due to the difficulty in distinguishing hyperpycnites from Bouma-type turbidites.

As shown in Table 3, on average, *ca* 40% of the facies associations in each section cannot be assigned confidently as Bouma-type turbidites or hyperpycnites. As mentioned before, hyperpycnites are characterized by typical inverse to normal grading (Figs 7, 8 and 17) or any sequences of sedimentary structures that indicate waxing and then waning flow energy (Figs 7 and 14). Under some conditions, the grading patterns cannot be determined and the basal inversely grading unit may be eroded, which makes it almost impossible to distinguish hyperpycnites from Bouma-type turbidites. Taking Fig. 8C as an example, one complete inversely to normally graded unit is separated by an undulating erosional surface (dashed line). However, towards the right of this sharp surface, the basal inversely graded part is totally eroded away, leaving only the normally graded part. In a second example, from 1.03 to 1.12 m in measured section 2, there are three event beds showing current ripple laminations that are separated by three bioturbated silty mudstone intervals (Fig. 13). Current ripple lamination can be produced from either surge-type turbidity currents or hyperpycnal flows. The bioturbation between beds in this example probably indicates three separate events. In other scenarios, Bouma-type turbidites cannot always be distinguished from hyperpycnites because it is not clear whether several beds stacked together represent deposition from one single event of sustained hyperpycnal flow (Lamb & Mohrig, 2009) or from several depositional events (stacked Bouma-type turbidites). In a third example, from 2.14 to 2.15 m in measured section 7 (shown as the schematic drawing in Fig. 18, log 13), three normally graded units are stacked. The grain size at the very bottom of each unit becomes coarser from the lower unit to the top one, suggesting an inverse-graded bedset. One possibility is that these three normally graded units are deposited from three successive surge-type turbidity currents. An alternative explanation

could be that these three beds are deposited from one hyperpycnal flow with internal velocity pulsing developed within the current itself (Kneller, 1995; Best *et al.*, 2005; Lamb *et al.*, 2008). Significant pauses between events should be marked by burrowed tops, but these could be eroded by successive events. In order for a bed to have a burrowed top, the time between events must be longer than the time needed to recolonize a substrate by infauna. Neoichnological theory suggests that this process might require several weeks to several months (MacEachern *et al.*, 2012). Amalgamated beds that lack burrows (i.e. the third example above) between events are thus likely to represent less than one year of deposition, and might lead towards interpretation as a sustained river-flooding event, versus decadal or centennial frequency floods. Bedsets in which bed-tops or intervening mudstones are burrowed are more likely to represent separate events (i.e. the second example above). Where events occur primarily at the decadal to centennial time frame, resulting in much lower sedimentation rates, and in areas unaffected by river discharge, robust, diverse and abundant trace-fossil suites will be the norm (MacEachern *et al.*, 2005). The overall sporadic patterns of bioturbation intensity and lack of robust trace fossils suggest that parasequence 6 is indeed deltaic in origin, and that flanking shorefaces also received river-derived prodelta mud, especially in the southern area. Because of the difficulty in distinguishing Bouma-type turbidites from hyperpycnites, and the possibility of storm-wave reworking of both of these, the importance of hyperpycnal flows may be underestimated in prodeltaic facies.

## CONCLUSION

- It is practical to quantify the relative importance of formative processes within each sedimentological section and determine the lateral variability in fluvial-dominated and wave-dominated processes within an ancient delta system through thin-bedded facies analysis.
- The variation in the relative proportion of sedimentary structures generated by fluvial-dominated and wave-dominated processes indicates a strong along-strike variation in parasequence 6–1 with a completely wave-dominated environment in the north (measured section 1; MS 1), passing abruptly into a fluvial-dominated, wave influ-



enced environment (measured sections 2 and 3; MS 2 and 3) southward, then to an environment with varying degrees of fluvial and wave influence southward (measured sections 4 to 7; MS 4 to 7), and back to a wave-dominated environment (measured sections 8 to 12; MS 8 to 12) further to the south-east. Based on this along-strike variation in dominant depositional processes and palaeocurrent data, parasequence 6–1 is interpreted to be a storm-dominated symmetrical delta with a large river-dominated bayhead system.

- Deltas are mixed-process systems. For deltaic environments that are dominated by a single process (river, wave or tide), the relative amounts of different depositional processes calculated from the thin-bedded facies (prodelta facies and distal delta front) and the sandy facies (proximal delta front, distributary channel or mouth-bar facies) above are consistent. In a mixed-process environment, however, consideration of only the sandy facies may not reflect the relative proportion of different depositional processes. The complex interactions between different depositional processes are more likely to be recorded more accurately by the thin-bedded prodelta facies and the heterolithic distal delta-front facies.

- Hyperpynites are characterized by typical inverse to normal grading or any sequences of sedimentary structures that indicate waxing and then waning flow energy. However, the relative proportion of hyperpynal flows calculated in this study seems to contradict the idea that the Ferron rivers were small and ‘dirty’, and commonly produced hyperpynal flows. This finding is probably because the basal inversely graded unit tends to be eroded, which leads to difficulties in distinguishing hyperpynites from amalgamated Bouma-type turbidites in the rock record; this suggests a preservational bias against hyperpynal flows, especially as sedimentation rates decrease.

## ACKNOWLEDGEMENTS

We thank reviewers Dr Christian Haug Eide and Dr Piret Plink-Björklund, and Associate Editor Dr Gary Hampson for their valuable comments and suggestions on the manuscript. We are grateful to the sponsors of University of Houston Quantitative Sedimentology Laboratories Consortium and Indiana University Shale Research Consortium (Anadarko, BHP Billiton, BP, Chevron, ConocoPhillips, EcoPetrol, ExxonMobil,

Inpex, Nexen, Pioneer, Shell, Statoil, Marathon, Whiting and Wintershall) for their generous financial support. We also thank Maria Love, Chenliang Wu, and Yangyang Li for their assistance in the field.

## REFERENCES

- Ahmed, S., Bhattacharya, J.P., Garza, D.E. and Li, Y. (2014) Facies architecture and stratigraphic evolution of a river-dominated delta front, Turonian Ferron Sandstone, Utah, U.S.A. *J. Sed. Res.*, **84**, 97–121.
- Ainsworth, R.B., Vakarelov, B.K. and Nanson, R.A. (2011) Dynamic spatial and temporal prediction of changes in depositional processes on clastic shorelines; toward improved subsurface uncertainty reduction and management. *AAPG Bull.*, **95**, 267–297.
- Arnott, R.W.C. (1993) Quasi-planar-laminated sandstone beds of the Lower Cretaceous Bootlegger Member, north-central Montana; evidence of combined-flow sedimentation. *J. Sed. Res.*, **63**, 488–494.
- Arnott, R.W. and Southard, J.B. (1990) Exploratory flow-duct experiments on combined-flow bed configurations, and some implications for interpreting storm-event stratification. *J. Sed. Res.*, **60**, 211–219.
- Barron, E.J. (1989) Severe storms during Earth history. *Geol. Soc. Am. Bull.*, **101**, 601–612.
- Best, J.L., Kostashuk, R.A., Peakall, J., Villard, P.V. and Franklin, M. (2005) Whole flow field dynamics and velocity pulsing within natural sediment-laden underflows. *Geology*, **33**, 765–768.
- Bhattacharya, J.P. (2011) Deltas. In: *Facies Model 4* (Eds N.P. James and R.W. Dalrymple), **84**, 233–264. SEPM Special Publication, Tulsa, OK.
- Bhattacharya, J.P. and Giosan, L. (2003) Wave-influenced deltas; geomorphological implications for facies reconstruction. *Sedimentology*, **50**, 187–210.
- Bhattacharya, J.P. and MacEachern, J.A. (2009) Hyperpynal rivers and prodeltaic shelves in the Cretaceous seaway of North America. *J. Sed. Res.*, **79**, 184–209.
- Bhattacharya, J.P. and Tye, R.S. (2004) Searching for modern Ferron analogs and application to subsurface interpretation. In: *The Fluvial-Deltaic Ferron Sandstone: Region to Wellbore-Scale Outcrop Analogs Studies and Application to Reservoir Modeling* (Eds T.C. Chidsey Jr, R.D. Adams and T.H. Morris), **50**, 39–57. AAPG Stud. Geol., Tulsa, OK.
- Bouma, A.H. (1962) *Sedimentology of Some Flysch Deposits; A Graphic Approach to Facies Interpretation*. Elsevier, Amsterdam/New York, 168 pp.
- Buatois, L.A., Santiago, N., Herrera, M., Plink-Björklund, P., Steel, R., Espin, M. and Parra, K. (2012) Sedimentological and ichnological signatures of changes in wave, river and tidal influence along a Neogene tropical deltaic shoreline. *Sedimentology*, **59**, 1568–1612.
- Campbell, C.V. (1967) Lamina, laminaset, bed and bedset. *Sedimentology*, **8**, 7–26.
- Charvin, K., Hampson, G.J., Gallagher, K.L. and Labourdette, R. (2010) Intra-parasequence architecture of an interpreted asymmetrical wave-dominated delta. *Sedimentology*, **57**, 760–785.
- Coates, L. and MacEachern, J.A. (2007) The ichnological signatures of river- and wave-dominated delta complexes;

- differentiating deltaic and non-deltaic shallow marine successions, Lower Cretaceous Viking Formation and Upper Cretaceous Dunvegan Formation, west-central Alberta. *SEPM Short Course Notes*, **52**, 227–254.
- Coleman, J.M. and Wright, L.D.** (1975) Modern river deltas; variability of processes and sand bodies. In: *Deltas, Models for Exploration* (Ed. M.L. Broussard), pp. 99–149. Houston Geological Society, Houston, TX.
- Dafoe, L.T., Gingras, M.K. and Pemberton, S.G.** (2010) Wave-influenced deltaic sandstone bodies and offshore deposits in the Viking Formation, Hamilton Lake area, south-central Alberta, Canada. *Bull. Can. Pet. Geol.*, **58**, 173–201.
- Ericksen, M.C. and Slingerland, R.L.** (1990) Numerical simulations of tidal and wind-driven circulation in the Cretaceous interior seaway of North America. *Geol. Soc. Am. Bull.*, **102**, 1499–1516.
- Felix, M., Peakall, J. and McCaffrey, W.D.** (2006) Relative importance of processes that govern the generation of particulate hyperpycnal flows. *J. Sed. Res.*, **76**, 382–387.
- Fielding, C.R.** (2010) Planform and facies variability in asymmetric deltas; facies analysis and depositional architecture of the Turonian Ferron Sandstone in the western Henry Mountains, south-central Utah, U.S.A. *J. Sed. Res.*, **80**, 455–479.
- Galloway, W.E.** (1975) Process framework for describing the morphologic and stratigraphic evolution of deltaic depositional systems. In: *Deltas, Models for Exploration* (Ed. M.L. Broussard), pp. 87–98. Houston Geological Society, Houston, TX.
- Gani, M.R. and Bhattacharya, J.P.** (2007) Basic building blocks and process variability of a Cretaceous delta; internal facies architecture reveals a more dynamic interaction of river, wave, and tidal processes than is indicated by external shape. *J. Sed. Res.*, **77**, 284–302.
- Gani, M.R., Bhattacharya, J. and MacEachern, J.A.** (2008) Using ichnology to determine relative influence of waves, storms, tides, and rivers in deltaic deposits: examples from Cretaceous Western Interior Seaway, USA. In: *Applied Ichnology* (Eds J.A. MacEachern, K.L. Bann, M.K. Gingras and S.G. Pemberton), *SEPM Short Course Notes*, **52**, 209–225.
- Garza, D.E.** (2010) *3-D Facies Architecture and Mouth Bar Development of a Flood-, Storm-dominated Delta: Cretaceous Ferron Sandstone, Utah*. University of Houston, Houston, TX, 67 pp.
- Hampson, G.J.** (2005) Sedimentologic and geomorphic characterization of ancient wave-dominated deltaic shorelines: Upper Cretaceous Blackhawk Formation, Book Cliffs, Utah, USA. In: *River Deltas – Concepts, Models, and Examples* (Eds L. Giosan and J.P. Bhattacharya), *SEPM Spec. Publ.*, **83**, 133–154.
- Hampson, G.J. and Storms, J.E.A.** (2003) Geomorphological and sequence stratigraphic variability in wave-dominated, shoreface-shelf parasequences. *Sedimentology*, **50**, 667–701.
- Hampson, G.J., Gani, M.R., Sharman, K.E., Irfan, N. and Bracken, B.** (2011) Along-strike and down-dip variations in shallow-marine sequence stratigraphic architecture; Upper Cretaceous Star Point Sandstone, Wasatch Plateau, Central Utah, U.S.A. *J. Sed. Res.*, **81**, 159–184.
- Hansen, C.D.** (2007) *Facies Characterization and Depositional Architecture of a Mixed-Influence Asymmetric Delta Lobe: Upper Cretaceous basal Belly River Formation, Central Alberta*. Simon Fraser University, Burnaby, 187 pp.
- Kneller, B.** (1995) Beyond the turbidite paradigm; physical models for deposition of turbidites and their implications for reservoir prediction. *Geol. Soc. Spec. Publ.*, **94**, 31–49.
- Lamb, M.P. and Mohrig, D.** (2009) Do hyperpycnal-flow deposits record river-flood dynamics? *Geology*, **37**, 1067–1070.
- Lamb, M.P., Myrow, P.M., Lukens, C., Houck, K. and Strauss, J.** (2008) Deposits from wave-influenced turbidity currents; Pennsylvanian Minturn Formation, Colorado, U.S.A. *J. Sed. Res.*, **78**, 480–498.
- Li, Y.** (2012) *Facies Architectural Study of Incised Valleys, Distributary Channels, and Mouth Bars in the Cretaceous Ferron Notom Delta, Southern Central Utah, USA*. University of Houston, Houston, TX, 176 pp.
- Li, W., Bhattacharya, J.P. and Campbell, C.** (2010) Temporal evolution of fluvial style in a compound incised-valley fill, Ferron 'Notom Delta', Henry Mountains Region, Utah (U.S.A.). *J. Sed. Res.*, **80**, 529–549.
- Li, W., Bhattacharya, J.P., Zhu, Y., Garza, D. and Blankenship, E.L.** (2011) Evaluating delta asymmetry using three-dimensional facies architecture and ichnological analysis, Ferron 'Notom Delta', Capital Reef, Utah, USA. *Sedimentology*, **58**, 478–507.
- Lock, B.E., Butler, R.W. and Franklund, R.T.** (2009) Tempestite sedimentation: an example from the Del Rio Formation of West Texas. *Trans GCAGS*, **59**, 463–476.
- MacEachern, J.A., Bann, K.L., Bhattacharya, J.P. and Howell, C.D., Jr** (2005) Ichnology of deltas; organism responses to the dynamic interplay of rivers, waves, storms, and tides. *SEPM Spec. Publ.*, **83**, 49–85.
- MacEachern, J.A., Dashtgard, S.E., Bann, K.L., Gingras, M.K., Zonneveld, J.P. and Pemberton, S.G.** (2012) The Ichnofacies Paradigm. In: *Trace Fossils as Indicators of Sedimentary Environments. Developments in Sedimentology* (Eds D. Knaust and R.G. Bromley), **64**, 103–138. Elsevier, Amsterdam.
- MacQuaker, J.H.S., Bentley, S.J. and Bohacs, K.M.** (2010) Wave-enhanced sediment-gravity flows and mud dispersal across continental shelves; reappraising sediment transport processes operating in ancient mudstone successions. *Geology*, **38**, 947–950.
- Mulder, T. and Chapron, E.** (2011) Flood deposits in continental and marine environments; character and significance. In: *Sediment Transfer from Shelf to Deep Water-Revisiting the Delivery System* (Eds R.M. Slatt and C. Zavala), **61**, 1–30. AAPG Studies in Geology, Tulsa, OK.
- Mulder, T. and Syvitski, J.P.M.** (1995) Turbidity currents generated at river mouths during exceptional discharges to the world oceans. *J. Geol.*, **103**, 285–299.
- Mulder, T., Migeon, S., Savoye, B. and Faugères, J.C.** (2001) Inversely graded turbidite sequences in the deep Mediterranean: a record of deposits from flood-generated turbidity currents? *Geo-Mar. Lett.*, **21**, 86–93.
- Mulder, T., Syvitski, J.P.M., Migeon, S., Faugeres, J.-C. and Savoye, B.** (2003) Marine hyperpycnal flows; initiation, behavior and related deposits; a review. *Mar. Pet. Geol.*, **20**, 861–882.
- Myrow, P.M. and Southard, J.B.** (1991) Combined-flow model for vertical stratification sequences in shallow marine storm-deposited beds. *J. Sed. Res.*, **61**, 202–210.



- Myrow, P.M., Fischer, W. and Goodge, J.W.** (2002) Wave-modified turbidites; combined-flow shoreline and shelf deposits, Cambrian, Antarctica. *Sed. Res.*, **72**, 641–656.
- Myrow, P.M., Lukens, C., Lamb, M.P., Houck, K. and Strauss, J.** (2008) Dynamics of a transgressive prodeltaic system; implications for geography and climate within a Pennsylvanian intracratonic basin, Colorado, U.S.A. *J. Sed. Res.*, **78**, 512–528.
- Normark, W.R. and Piper, D.J.W.** (1991) Initiation processes and flow evolution of turbidity currents; implications for the depositional record. In: *From Shoreline to Abyss: Contributions in Marine Geology in Honor of Francis Parker Shepard* (Ed. R.H. Osborne), *SEPM Spec. Publ.*, **46**, 207–230.
- Parsons, J.D., Bush, J.W.M. and Syvitski, J.P.M.** (2001) Hyperpycnal plume formation from riverine outflows with small sediment concentrations. *Sedimentology*, **48**, 465–478.
- Passey, Q.R., Dahlberg, K.E., Sullivan, K.B., Yin, H.R., Brackett, A., Xiao, Y.H. and Guzman-Garcia, A.G.** (2006) Definitions and geologic occurrence of thin beds in clastics. In: *Petrophysical Evaluation of Hydrocarbon Pore-thickness in Thinly Bedded Clastic Reservoirs* (Ed. Q.R. Passey), *AAPG Archie Series*, Tulsa, OK, 27–39.
- Piper, D.** (1978) Turbidite muds and silts on deep sea fans and abyssal plains. In: *Sedimentation in Submarine Canyons, Fans and Trenches* (Eds D.J. Stanley and G. Kelling), pp. 163–176. Dowden, Hutchinson & Ross, Stroudsburg.
- Plink-Björklund, P. and Steel, R.J.** (2004) Initiation of turbidity currents: outcrop evidence for Eocene hyperpycnal flow turbidites. *Sed. Geol.*, **165**, 29–52.
- Plint, A.G.** (2014) Mud dispersal across a Cretaceous prodelta; storm-generated, wave-enhanced sediment gravity flows inferred from mudstone microtexture and microfacies. *Sedimentology*, **61**, 609–647.
- Reading, H.G. and Collinson, J.** (1996) Clastic coasts. In: *Sedimentary Environments: Processes, Facies and Stratigraphy* (Ed. H.G. Reading), pp. 154–231. Blackwell, Oxford, UK.
- Ricci Lucchi, F. and Valmori, E.** (1980) Basin-wide turbidites in a Miocene, over-supplied deep-sea plain: a geometrical analysis. *Sedimentology*, **27**, 241–270.
- Schieber, J.** (1999) Distribution and deposition of mudstone facies in the Upper Devonian Sonyea Group of New York. *J. Sed. Res.*, **69**, 909–925.
- Seepersad, D.** (2012) *Thin-bedded Facies Analysis of a Ferron Storm-dominated Delta Front and Prodelta: Cretaceous Ferron Sandstone, Utah*. University of Houston, Houston, TX, 98 pp.
- Slingerland, R. and Keen, T.R.** (1999) Sediment transport in the Western Interior Seaway of North America; predictions from a climate-ocean-sediment model. In: *Isolated Shallow Marine Sand Bodies* (Eds K.M. Bergman and J.W. Snedden), *SEPM Spec. Publ.*, **64**, 179–190.
- Slingerland, R., Kump, L.R., Arthur, M.A., Fawcett, P.J., Sageman, B.B. and Barron, E.J.** (1996) Estuarine circulation in the Turonian-Western Interior Seaway of North America. *Geol. Soc. Am. Bull.*, **108**, 941–952.
- Stow, D.A.V. and Shanmugam, G.** (1980) Sequence of structures in fine-grained turbidites; comparison of Recent deep-sea and ancient flysch sediments. *Sed. Geol.*, **25**, 23–42.
- Swift, D.J.P. and Nummedal, D.** (1987) Hummocky cross-stratification, tropical hurricanes and intense winter storms. *Sedimentology*, **34**, 338–344.
- Talling, P.J., Masson, D.G., Sumner, E.J. and Malgesini, G.** (2012) Subaqueous sediment density flows; depositional processes and deposit types. *Sedimentology*, **59**, 1937–2003.
- Taylor, A.M. and Goldring, R.** (1993) Description and analysis of bioturbation and ichnofabric. *J. Geol. Soc. London*, **150**, 141–148.
- Wheatcroft, R.A.** (2000) Oceanic flood sedimentation: a new perspective. *Cont. Shelf Res.*, **20**, 2059–2066.
- Zhu, Y., Bhattacharya, J.P., Li, W., Lapen, T.J., Jicha, B.R. and Singer, B.S.** (2012) Milankovitch-scale sequence stratigraphy and stepped forced regressions of the Turonian Ferron Notom deltaic complex, south-central Utah, U.S.A. *J. Sed. Res.*, **82**, 723–746.

*Manuscript received 4 March 2015; revision accepted 28 May 2015*